MAGNETIC FIELD ASSISTED FINISHING OF ULTRA-LIGHTWEIGHT AND HIGH-RESOLUTION MEMS X-RAY MICRO-PORE OPTICS

By

RAÚL EDUARDO RIVEROS

A THESIS PRESENTED TO THE GRADUATE SCHOOL
OF THE UNIVERSITY OF FLORIDA IN PARTIAL FULFILLMENT
OF THE REQUIREMENTS FOR THE DEGREE OF
MASTER OF SCIENCE

UNIVERSITY OF FLORIDA

2009

© 2009 Raúl Eduardo Riveros

To my family.

ACKNOWLEDGMENTS

I would like to thank my parents, as I would be nothing without their everlasting dedication, support, teachings, and love. I would also like to thank my awesome advisor, Dr. Hitomi Yamaguchi Greenslet, for believing in and working with me; I believe it is a great honor to work with her. I would like to thank the Dr. Tony L. Schmitz who graciously welcomed me into his lab and assigned me to projects which readied me for my graduate study. I also want to thank Dr. John K. Schueller for letting me into graduate school and being on my committee.

I wish to thank our partners in Japan, Dr. Yuichiro Ezoe, Ikuyuki Mitsuishi, Masaki Koshiishi, Utako Tagaki and Fumiki Kato, for their great efforts in coordinating and realizing our goals. A special thanks goes to Dr. John Greenslet, who very kindly edited my written work. I want to thank all members of the Machine Tool Research Center, particularly those present from July 2006 to May 2009; we will all be best friends forever (BFF).

TABLE OF CONTENTS

page

ACKNOWLEDGMENTS 4

LIST OF TABLES 7

LIST OF FIGURES 8

ABSTRACT 11

CHAPTER

1 INTRODUCTION 13

1.1 X-Ray Astronomy 13
1.2 Background 13
1.2.1 Reflection and Refraction of Electromagnetic Radiation 13
1.2.2 X-Ray Reflection 15
1.3 X-Ray Telescopes 16
1.3.1 Wolter Type-I Optics 17
1.3.2 Technical Issues of Existing Wolter Type-I Optics 18
1.4 X-Ray Mirror Fabrication Technologies 19
1.4.1 Glass Sheet Mirrors 19
1.4.2 Thin Foil Mirrors 20
1.4.3 Micro-Pore Mirrors 20
1.5 MEMS Type X-Ray Mirror Fabrication 21
1.5.1 Anisotropic Wet Etching 21
1.5.2 Deep Reactive Ion Etching (DRIE) 22
1.5.3 X-Ray Lithography (LIGA) 24

2 MAGNETIC FIELD ASSISTED FINISHING 26

2.1 Introduction to Magnetic Field Assisted Finishing 26
2.2 Static Magnetic Field Assisted Process 30
2.3 Alternating Magnetic Field Assisted Process 32

3 DEVELOPMENT OF PROCESS PRINCIPLE AND POLISHING MACHINE . 34

3.1 Micro-Pore X-Ray Mirrors 34
3.2 Processing Principle for Micro-Pore X-Ray Mirror Polishing 38
3.3 Design Concept and Specifications of Polishing Machine 40
3.4 Polishing Machine 40
3.4.1 Design and Build 40
3.4.2 Dynamic Motion of Ferrous Slurry 43

4 POLISHING CHARACTERISTICS 49

4.1 Surface Roughness Analysis 49
4.2 Experimental Procedure 51
4.3 DRIE-Fabricated Mirrors 53
4.3.1 Unpolished State 53
4.3.2 Effects of Diamond Slurries on Polishing Characteristics 55
4.3.3 Effects of Polishing Time on Polishing Characteristics 55
4.3.4 Effects of Frequency of Magnetic Field on Polishing Characteristics 57
4.3.5 Effects of Micro-pore Width on Polishing Characteristics 59
4.3.6 Effects of Chemical Assistance on Polishing Characteristics 60
4.4 LIGA-Fabricated Mirrors 63
4.4.1 Unpolished State 63
4.4.2 Polishing Characteristics 65

5 X-RAY REFLECTION TESTING 67

5.1 Testing Method 67
5.2 Grazing Incidence X-Ray Scattering and Specular Reflectance Test Results 68

6 CONCLUSIONS 70

6.1 Concluding Statements 70
6.2 Future Work 70

APPENDIX: TESTING PLAN 73

REFERENCES 76

BIOGRAPHICAL SKETCH 78

LIST OF TABLES

Table		page
3-1	Machine specifications.	42
4-1	Experimental conditions for abrasive size test.	55
4-2	Experimental conditions for polishing time test.	57
4-3	Experimental conditions for oscillating frequency test.	58
4-4	Experimental conditions for micro-pore width test.	60
4-5	Experimental conditions for chemical assistance test.	62
4-6	Experimental conditions for nickel mirror chip trial.	65
A-1	Experimental conditions for each test on silicon mirror chips.	74
A-2	Silicon mirror chips used for testing and their micro-pore dimensions.	75
A-3	Surface roughness values of silicon mirror chip micro-pore sidewalls	75

LIST OF FIGURES

Figure page

1-1 Schematic of the electromagnetic spectrum. 13

1-2 Schematic of a wave reflecting and refracting off a surface. 14

1-3 Schematic of generic optical focusing. 17

1-4 Schematic of Wolter type-I mirror arrangement. 18

1-5 Schematic of a cut-away view of a Wolter type-I nested mirror arrangement. . . 18

1-6 A simple diagram of nested annular rings. 19

1-7 Comparison between glass/foil mirror type mirrors and micro-pore mirrors. . . . 21

1-8 Schematic of wet etching process flow. 22

1-9 Schematic of DRIE process flow. 23

1-10 Schematic of DRIE etching mechanism. 23

1-11 X-ray LIGA process flow. 25

2-1 Schematic of a standard wafer polishing machine. 27

2-2 Schematic of a wafer polishing process modified to use MAF. 28

2-3 Schematic of processing principle for static magnetic field polishing process. . . 31

2-4 Photograph of static magnetic field assisted internal finishing equipment. 31

2-5 Schematic of processing principle for alternating magnetic field assisted machining process. 33

2-6 Photograph of alternating magnetic field assisted machining equipment. 33

3-1 Photograph of a silicon single stage Wolter type I optic. 34

3-2 Schematic of the function of a micro-pore x-ray mirror. 35

3-3 Photograph of a silicon mirror chip. 36

3-4 Photograph of a nickel mirror chip. 37

3-5 Photograph of a LIGA mold for electroplating. 37

3-6 Size comparison between a full optic and a mirror chip. 38

3-7 Two-dimensional schematic of processing principle. 41

3-8 CAD design of polishing machine. 42

3-9 Magnetic circuit. 43
3-10 Photograph of completed polishing machine. 44
3-11 Workstation setup. 44
3-12 Original electric circuit and a two-dimensional schematic of the corresponding fluid behavior. 45
3-13 Fluid motion using original circuit. 46
3-14 Modified circuit and current plot. 47
3-15 Two-dimensional schematic of fluid behavior with modified circuit design. 47
3-16 Fluid motion using modified circuit. 48
3-17 Schematic of transient states of magnetic field during operation. 48
4-1 Schematic of a surface profile. 49
4-2 Schematic of a surface profile broken down into waviness and roughness. 50
4-3 Photograph of experimental setup with a mirror chip mounted. 52
4-4 Micrograph of an unpolished DRIE-fabricated mirror chip micro-pore sidewall. . 54
4-5 Three-dimensional shape of unpolished silicon mirror chip sidewall surface measured by an optical profilometer. 54
4-6 Surface roughness results from abrasive size tests. 56
4-7 Three-dimensional shape of silicon mirror chip micro-pore sidewall surfaces after abrasive size testing as measured by an optical profilometer. 56
4-8 Surface roughness results from polishing time tests. 57
4-9 Three-dimensional shape of silicon mirror chip micro-pore sidewall surfaces after polishing time testing as measured by an optical profilometer. 58
4-10 Surface roughness results from frequency variation tests. 59
4-11 Three-dimensional shape of silicon mirror chip micro-pore sidewall surfaces after frequency variation testing as measured by an optical profilometer. 59
4-12 Surface roughness results from micro-pore width tests. 61
4-13 Three-dimensional shape of silicon mirror chip micro-pore sidewall surfaces after micro-pore width variation testing as measured by an optical profilometer. . . . 61
4-14 Surface roughness results from chemical assistance tests. 63

4-15 Three-dimensional shape of silicon mirror chip micro-pore sidewall surfaces after chemical assistance testing as measured by an optical profilometer. 64

4-16 Optical profilometer data for an unpolished mirror chip. 64

4-17 Optical profilometer data for a polished mirror chip. 66

4-18 Comparison of sidewall surface roughness before and after polishing. 66

5-1 Schematic of x-ray reflectance testing setup for micropore mirror chips. 67

5-2 X-ray reflectance testing setup. 68

5-3 X-ray reflectance data for a polished nickel mirror chip. 69

Abstract of thesis Presented to the Graduate School
of the University of Florida in Partial Fulfillment of the
Requirements for the Degree of Master of Science

MAGNETIC FIELD ASSISTED FINISHING OF ULTRA-LIGHTWEIGHT AND HIGH-RESOLUTION MEMS X-RAY MICRO-PORE OPTICS

By

Raúl Eduardo Riveros

May 2009

Chair: Hitomi Yamaguchi Greenslet
Major: Mechanical Engineering

In recent years, x-ray telescopes have been shrinking in both size and weight to reduce cost and volume on space flight missions. Current designs focus on the use of micro-electro-mechanical systems (MEMS) technologies to fabricate ultra-lightweight and high-resolution Wolter type I x-ray optics. In 2006, Ezoe *et al.* introduced micro-pore x-ray optics fabricated using anisotropic wet etching of silicon (110) wafers. These optics, though lightweight (complete telescope weight less than 1 kg for an effective area of 1000 cm^2), had limited angular resolution, as the reflecting surfaces were flat crystal planes. To achieve higher angular resolution, curved micro-pores are required.

Two MEMS techniques were used to fabricate x-ray optics with curvilinear micro-pores; however, the resulting curved sidewalls were too rough to reflect x-rays. To solve this issue, an ultra-precision polishing process employing alternating magnetic field assisted finishing was proposed. A processing principle was devised using a magnetic abrasive fluid mixture and an alternating and switching magnetic field. The concept involves two coaxial, inward facing, magnetic poles. The micro-pore optic is submerged in the fluid mixture and placed between the poles. The fluid mixture oscillates from pole to pole, flowing through the optic's micro-pores, thus polishing the sidewalls. A machine was constructed to realize this principle on miniature workpieces called mirror chips (7.5 mm^2 wafers with micro-pores). The effects on sidewall roughness of several process parameters were studied; this demonstrated the feasibility of the proposed process to

obtain a micro-pore sidewall roughness of less than 5 nm *rms*. The x-ray reflectance of the polished mirror chips was also confirmed.

CHAPTER 1
INTRODUCTION

1.1 X-Ray Astronomy

X-ray emission from celestial objects such as black holes, binary star systems, white dwarf, neutron stars, and other star types cannot be studied on earth due to atmospheric absorption. Therefore, the study of such high energy emitting objects must occur above the atmosphere in space. Since the 1960s, x-ray telescopes have been launched into space and the field of x-ray astronomy has rapidly developed since then. Data from x-ray telescopes have given astrophysicists new challenges and have prompted new theories about particle physics and the structure and origin of the universe[1].

In December 2008, Ezoe *et al.* presented the development of a new class of x-ray optics which would allow for the construction of ultra-lightweight and high resolution x-ray telescopes[2]. Dr. Yuichiro Ezoe's high-energy astrophysics research group at the Japan Aerospace Exploration Agency (JAXA) is collaborating with Hitomi Yamaguchi and Raul E. Riveros at the University of Florida. The purpose of this collaboration is to produce an ultra-lightweight and high resolution x-ray telescope.

1.2 Background

1.2.1 Reflection and Refraction of Electromagnetic Radiation

Electromagnetic radiation (EMR) interacts with matter differently depending how much energy the radiation possesses. EMR is classified into different groups by wavelength as shown in Figure 1-1.

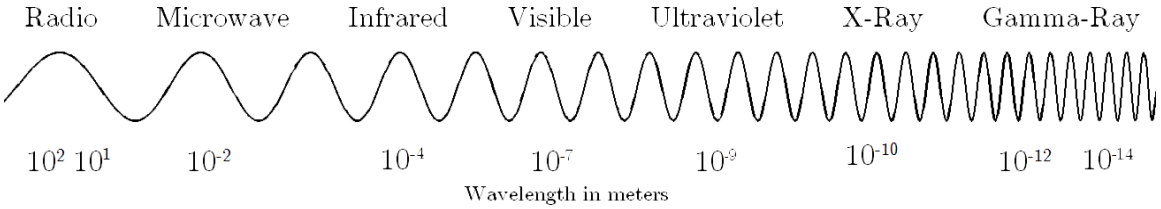

Figure 1-1. Schematic of the electromagnetic spectrum.

When a ray of EMR strikes a surface, it either reflects, refracts, is absorbed, or all three. These interactions are complex phenomena with many factors at play, though, to attain a simple understanding of this phenomenon, only a few of those factors require consideration. The first factor needing attention is the refractive index of the medium through which a wave passes. The refractive index of a material is the ratio of a wave's phase velocity through a reference medium (speed of light in a vacuum) to the phase velocity through the medium at hand. This relationship is shown in the following equation:

$$n = \frac{c}{v} \tag{1–1}$$

where c is the phase velocity of the wave through a reference medium and v is wave's phase velocity through the medium with which it is interacting. The phase velocity, and thus the refractive index, of a wave through a medium depends on both the medium's properties such as the atomic scattering factor and density and the wave's properties such as its energy and electric-field vector orientation[3].

Figure 1-2 shows a wave impinging on a surface and two components, the reflected wave and the refracted wave. Snell's law relates the refractive indices of mediums through

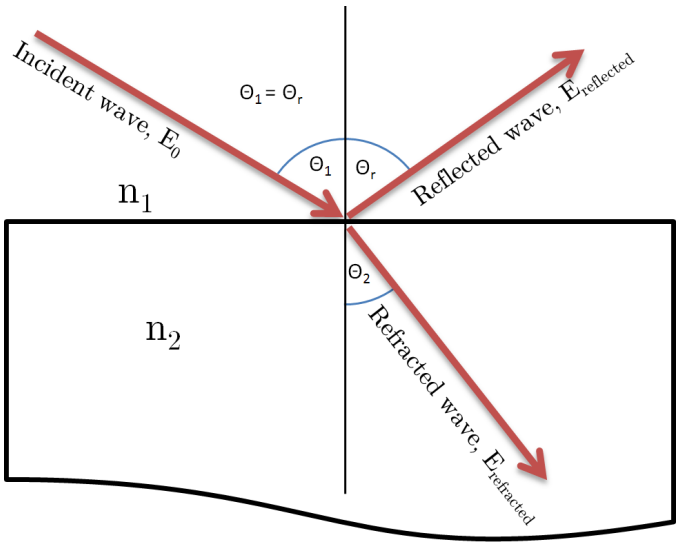

Figure 1-2. Schematic of a wave reflecting and refracting off a surface.

which a wave travels and the incident and refracted wave angles; it is presented here:

$$n_1 \sin\theta_1 = n_2 \sin\theta_2 \tag{1–2}$$

where n_1 and n_2 are the refractive indices of two adjacent mediums and θ_1 and θ_2 are the incident and refracted wave angles. As the angle of incidence, θ_1, increases, a phenomenon known as total internal reflection occurs. At a certain critical angle, θ_c, the wave ceases to refract into the adjacent medium and completely reflects. Total internal reflection only occurs if the medium in which the wave is originally in has a higher refractive index than the adjacent medium ($n_1 > n_2$). The critical angle is found by rewriting Snell's law (1–2) and setting $\theta_2 = 90°$[3].

$$\sin\theta_c = \frac{n_2}{n_1}$$
$$\theta_c = \arcsin\frac{n_2}{n_1} \tag{1–3}$$

Total external reflection is a term often used to identify the total reflection of a wave off a surface. The wave, in this case, is typically traveling through a vacuum. It is the same phenomenon as total internal reflection; however, the term *external* implies that the wave initially travels from the surroundings of the reflection interface.

1.2.2 X-Ray Reflection

X-rays are a high energy form of EMR. The refractive index for a medium interacting with x-ray radiation is typically calculated using the following formula:

$$n = 1 - \delta - i\beta = 1 - \frac{r_0\lambda^2}{2\pi}N_{at}(f_1 - if_2) \tag{1–4}$$

where δ is difference between the refractive index and 1, β is the material's absorption index, f_1 and f_2 are the real and imaginary components of the material's atomic scattering factor, N_{at} is the material's atomic density (atoms per unit volume), r_0 is the radius of an electron, i is the imaginary number, and λ is the wavelength of the x-ray radiation[4].

It happens that all materials have refractive indices slightly less than 1 for x-rays. Such values for refractive indices indicate that x-ray reflection and refraction is not as

easily achievable as with lower energy EMR. In fact, x-rays are, at least partially, absorbed by all materials[4].

Imaging x-rays has historically been challenging. Because most materials have refractive indices just slightly below 1, lenses are impractical as focal lengths would be extremely long. Practically, the most efficient way to change the direction of an x-ray is through total external reflection. X-ray lenses are designed to employ the total external reflection of x-rays so as to focus them to a point onto a detector for imaging. There are many designs in existence; however, the design of x-ray telescopes operating in outer space is relevant to this document.

1.3 X-Ray Telescopes

Early (1960s) x-ray telescope designs simply had a large area detector and a collimator, only able to image x-ray signals which entered the device parallel to the collimator. To increase the sensitivity of telescopes, x-ray optics in telescope designs were needed. Due to the difficulty involved with focusing x-rays, the optics underwent much development[5].

X-ray optics should be able to properly focus x-rays efficiently without distorting the incoming x-ray radiation such that the detected image accurately represents the incoming signals. In theory, reflection off a perfectly flat and smooth surface produces specular reflection (clear, undistorted). Reflection off a rough surface would produce diffuse reflection (blurred, distorted). In practice, total external reflection is difficult to achieve due to the roughness of the reflecting surfaces. Thus, to maximize the reflecting capability of a surface it should achieve as much specular reflection as possible and have maximum reflected wave intensity. To achieve specular reflection, the reflecting surfaces must be as smooth as possible. To maximize the intensity of the reflected wave, the angle of incidence should be as large as technically possible. Such extremely incidence angles are known as grazing incidence.

In order for an optic system, as shown in Figure 1-3, to successfully form an image, its geometric arrangement must satisfy the Abbe sine condition, stated in (1–5).

$$\frac{h}{\sin\alpha} = r \tag{1–5}$$

This equation must be true or nearly true for proper image formation. Therefore, a functional x-ray optical system must not only achieve efficient x-ray reflection, but it must also satisfy the Abbe sine condition[5].

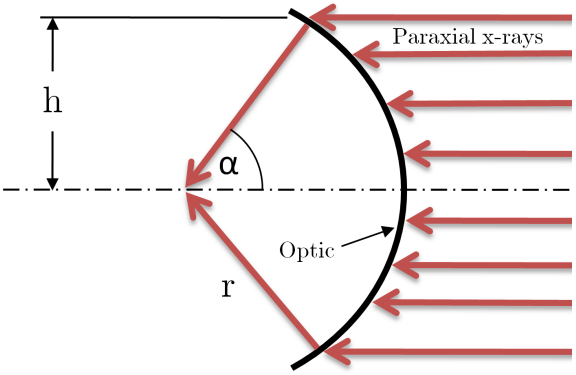

Figure 1-3. Schematic of generic optical focusing.

1.3.1 Wolter Type-I Optics

In 1952, Hans Wolter, a German physicist, proposed three x-ray optic designs with curved mirrors whose surfaces coincide with a paraboloid and another set whose surfaces coincide with a hyperboloid. Of the three designs, one has been the most practical for x-ray telescopes. Figure 1-4 shows Wolter's type-I x-ray optical arrangement. This arrangement not only allows for total external reflection off the reflecting surfaces but also nearly satisfies the Abbe condition. The upper mirrors are contoured to follow a paraboloid while the lower mirrors are contoured to follow a confocal hyperboloid. In actuality, telescopes contain many nested layers of mirrors as shown in Figure 1-5. Such an arrangement allows for greater detection area[5].

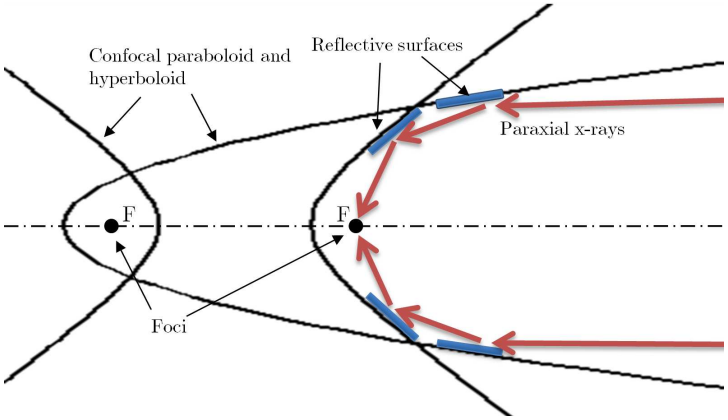

Figure 1-4. Schematic of Wolter type-I mirror arrangement.

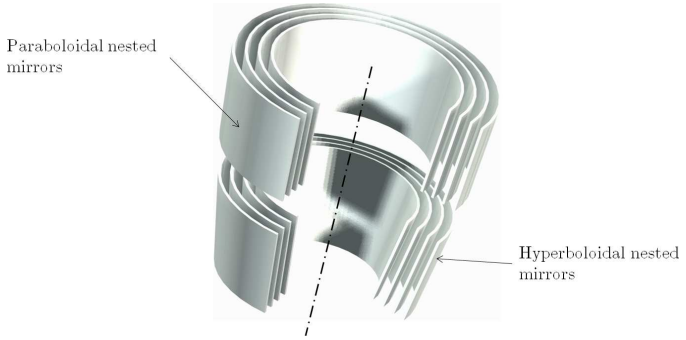

Figure 1-5. Schematic of a cut-away view of a Wolter type-I nested mirror arrangement.

1.3.2 Technical Issues of Existing Wolter Type-I Optics

There exist many technical issues with the construction of Wolter type-I optics. The first major issue is that Wolter type-I telescopes form a discontinuous image. If the telescope contained only one paraboloidal mirror and one hyperboloidal mirror, it would be capable of imaging a single annular region. Nesting sets of mirrors simply adds more coaxial but separate annular regions of a decreasing diameter to the captured image. This nesting of annular regions is shown in Figure 1-6. The area between the black annular regions in Figure 1-6 is due to the thickness of the reflecting surfaces. The thickness of the reflecting surfaces causes a radial discontinuity in the captured image. Also, support structures for the inner nested mirror sets cause angular discontinuities as well.

The next major technical issue is weight. X-ray telescopes intended for astrophysics research must operate in outer space. Thus, they need to be transported by a rocket. The

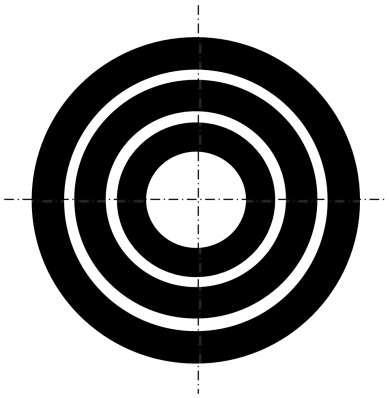

Figure 1-6. A simple diagram of nested annular rings.

cost per unit weight for transporting a satellite into space is extremely high ($10K per kg); therefore, it is important that the telescope be as light as possible. Existing Wolter type-I x-ray telescopes tend to be large and heavy, for they require precise hardware and support structures.

1.4 X-Ray Mirror Fabrication Technologies

To minimize the total area of discontinuities in the image formed from Wolter type-I optics, the thickness of the reflecting surfaces is minimized. Reducing this thickness also results in a reduction in weight. The thickness the reflecting surfaces and weight of x-ray telescopes that have actually gone into service has greatly reduced in the past decade. The fabrication of the optics has evolved from using polished and coated contoured glass sheets to very thin and lightweight contoured gold foils. However, the most recent designs involve micro-pore optical devices which promise high resolution and ultra-lightweight x-ray optics fabricated by micro-fabrication techniques common to the semiconductor industry. These fabrication methods will be described in detail in the following subsections.

1.4.1 Glass Sheet Mirrors

Glass sheet type of mirror is made by first molding small glass sheets, and then polishing and coating them. This type of mirror was used on the Chandra x-ray observatory. The optics on this satellite achieved an excellent angular resolution of 0.5 arc seconds as they were formed to have a paraboloidal surface. However, it rendered a

large and heavy telescope assembly. The mirror assembly's diameter was 120 cm and was 85 cm deep. The completed mirror assembly weighed 950 kg[6].

1.4.2 Thin Foil Mirrors

Foil type mirrors are made from thin sheets of coated aluminum which is then heated and formed over a mandrel. This type of mirror was used on the Japanese Suzaku x-ray observatory. The mirror assemblies on Suzaku measured 40 cm in diameter and 120 cm deep. The optics on this satellite had an angular resolution of about 100 arc seconds. The reduction in angular resolution is due to the fact that the foils did not have a paraboloidal surface. Instead, the foils were conical, as they were easier to produce. Designers of the Suzaku observatory attempted to counter act the paraboloidal shape by including a larger number of reflecting surfaces. Although Suzaku's resolution is considerably less than Chandra's, the weight savings were superb. The entire mirror assembly weighed in at just 19 kg[7].

1.4.3 Micro-Pore Mirrors

In a continuing effort to reduce the weight of x-ray telescopes, micro-pore optics are to be used. Micro-pore optics are used to focus x-rays from sources on earth. Figure 1-7 shows a comparison between micro-pore and glass/foil type mirrors. Essentially, these optics consist of a substrate with through-pores; the pore sidewalls are intended for use as grazing incidence mirrors. Reduced reflecting surface thickness will allow for better imaging. Micro-pore optics, if realized, could allow for the construction of fully capable x-ray telescopes weighing approximately 1 kg[8].

Micro-pore x-ray optics are fabricated using techniques commonly used for the manufacturing of micro-electro-mechanical systems (MEMS). There are three techniques which can be most useful for creating micro-pore x-ray optics; they will be described in the next section.

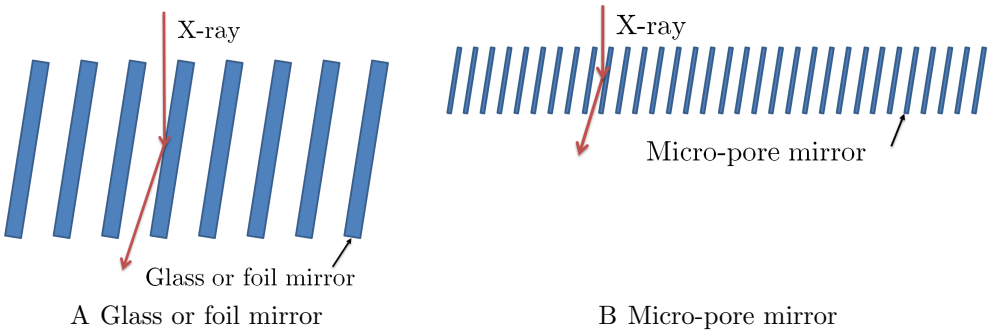

Figure 1-7. Comparison between glass/foil mirror type mirrors and micro-pore mirrors.

1.5 MEMS Type X-Ray Mirror Fabrication

The goal of using these MEMS fabrication methods is to render micro-pore optics capable of imaging x-ray signals from deep space. To accomplish this goal, the micro-pore sidewalls should be able to achieve total external reflection of incoming x-rays, meaning that the reflecting surfaces should be < 1 nm *rms*. Unfortunately, there is currently no way to create paraboloidal reflecting surfaces in micro-pore optics. This will limit the resolution of the telescope; however, as with the Suzaku telescope, an increased number of reflecting surfaces will improve the telescope's resolution, and micro-pore optics are capable of having an extremely high number of reflecting surfaces. The different MEMS manufacturing methods applicable to the fabrication micro-pore x-ray optics will be discussed in the following subsections.

1.5.1 Anisotropic Wet Etching

The wet etching process flow is shown in Figure 1-8. The wet etching of silicon involves coating a silicon wafer with either silicon nitride or silicon oxide on both sides (top and bottom). A layer of photoresist is placed on the top coat. Using ultraviolet radiation (UV) and a UV mask, the coating on the top layer is exposed to the UV radiation. The photoresist is then developed and the top layer of silicon nitride/oxide is etched. The remaining photoresist is removed and the silicon wafer is now masked only by

the etched coating. Using KOH solution, the silicon is etched and the coating layers are then removed, exposing the silicon.

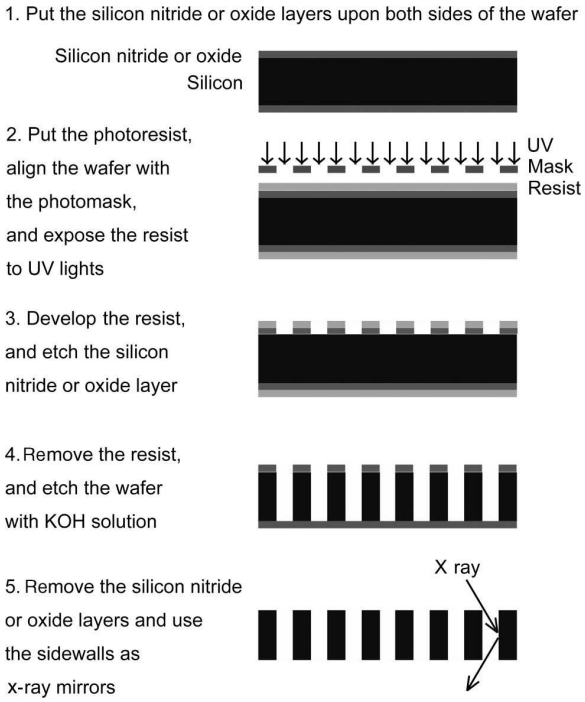

Figure 1-8. Schematic of wet etching process flow. [Courtesy of Yuichiro Ezoe]

This type of etching is anisotropic. This limits it to etching only straight trenches along the silicon's crystal planes, rendering only straight micro-pores. Ezoe *et al.* presented micro-pore optics made using this wet etching technique. In their effort, an ultrasonic wave was used during the etching of the silicon to improve the resulting micro-pore sidewall roughness to less than 1 nm *rms*. These optics therefore had excellent specular reflection of x-rays; however, they had limited angular resolution as the reflecting surfaces were flat planes which does not comply with a true Wolter type-I optic design[8].

1.5.2 Deep Reactive Ion Etching (DRIE)

DRIE is a MEMS fabrication technique capable of producing curvilinear micro-pores in a silicon substrate. The overall process flow is no different from a standard etching process. The process flow is shown in Figure 1-9. A layer of photoresist is placed on a silicon wafer. Using a UV mask and UV radiation, the mask is exposed to the UV. The

resist is developed and then the DRIE process etches the silicon substrate. The photoresist is later removed using an ultrasonic cleaner.

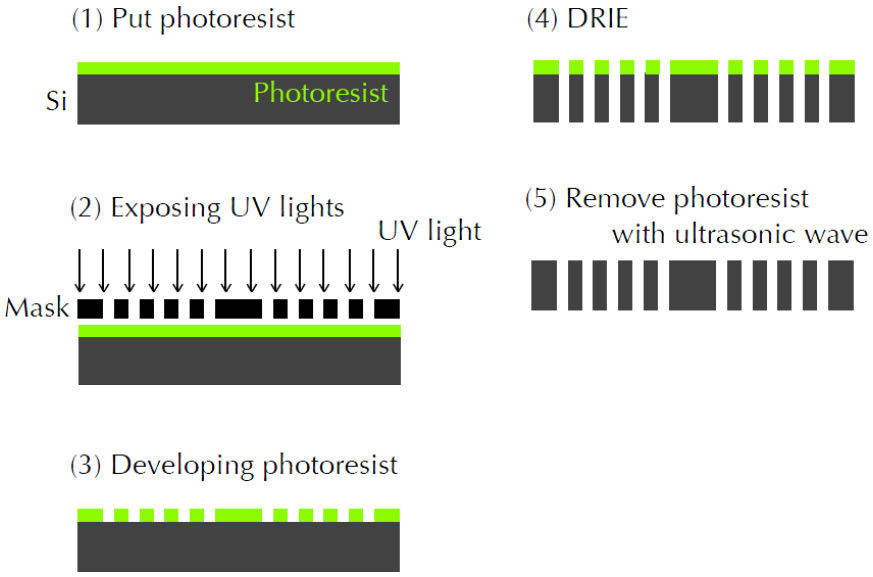

Figure 1-9. Schematic of DRIE process flow.

The actual DRIE mechanism has two phases as shown in Figure 1-10. First, the silicon is exposed to fluorine ions which react with the silicon and create SiF_4 gas, this is called the "Etching Mode". Then the exposed silicon is coated in a $(-CF_2-)$ polymer, this is called the "Passivation Mode". This polymer coating protects the trench sidewalls from further etching and undercutting. The process is then repeated until the desired etching depth is reached.

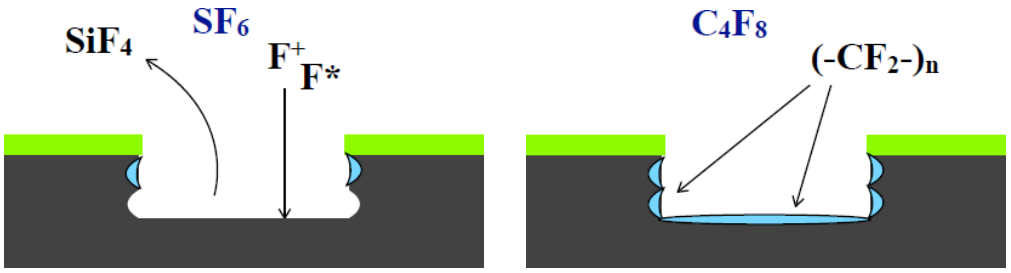

Figure 1-10. Schematic of DRIE etching mechanism.

There are several advantages to using DRIE. The different process parameters can be tweaked to optimize the process for speed, geometry, or sidewall roughness. It is also capable of producing any pattern and can create structures with very high aspect ratios. DRIE's main limitation regarding the fabrication of micro-pore optics is the sidewall geometry[9]. DRIE requires extensive optimization to achieve straight sidewalls and a sidewall roughness that yields adequate specular reflection of x-rays.

1.5.3 X-Ray Lithography (LIGA)

X-ray lithography (LIGA) is a micro-fabrication technique developed in Germany. LIGA is a German acronym: **Li**thographie (Lithography), **G**alvanoformung (Electroforming), and **A**bformung (Molding). The process, as shown in Figure 1-11 begins with a sheet of polymethyl methacrylate (PMMA) and a mask capable of obscuring x-rays. The mask is placed over the PMMA substrate and the setup is exposed to synchrotron radiation, namely high energy (hard) x-rays. The radiation tends to destroy the PMMA structure. The affected areas are then removed with a chemical solution[10]. The mold produced from these steps is then sputtered with a 50 nm thick layer of gold. The sputtered mold is then electro plated with nickel. The electroplated mold is then ground on both sides to render the nickel structure with the remaining PMMA through the thickness. The remaining PMMA is then dissolved and only the nickel is left.

There are some advantages to fabricating microstructures with LIGA as opposed to etching. LIGA allows for the production of high aspect ratio structures. Also the side walls of features are very straight and typically have a surface roughness of about 10 nm *rms*[11]. Also, both nickel and gold are materials commonly used for x-ray reflecting surfaces.

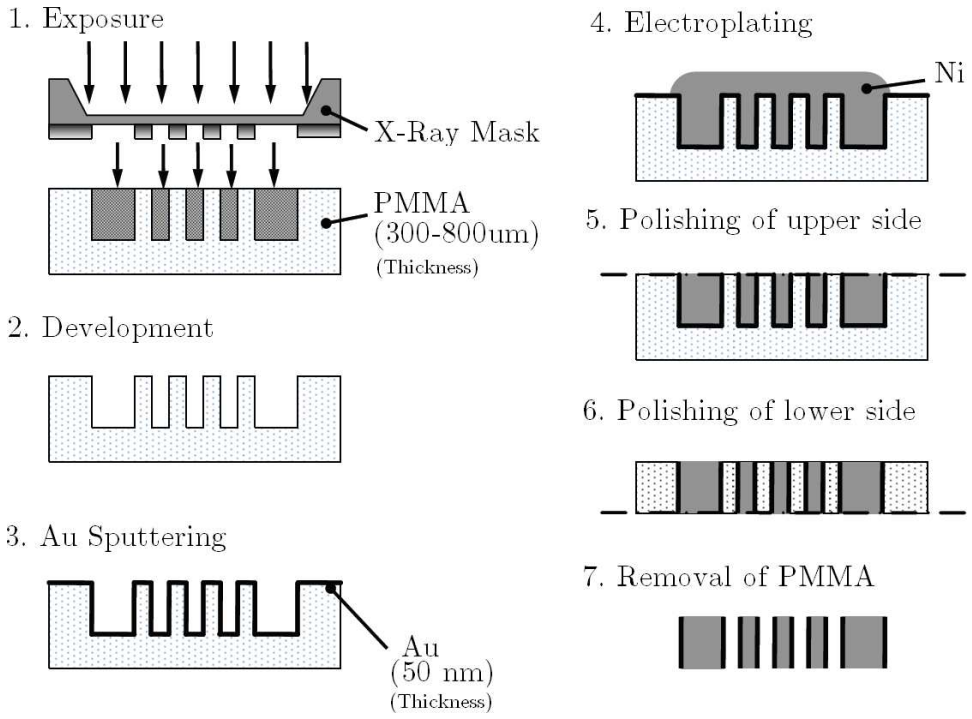

Figure 1-11. LIGA process flow. [Courtesy of Yuichiro Ezoe]

CHAPTER 2
MAGNETIC FIELD ASSISTED FINISHING

2.1 Introduction to Magnetic Field Assisted Finishing

Magnetic field assisted finishing (MAF) is a type of finishing process in which abrasive particles are either directly or indirectly actuated onto a workpiece by magnetic force, as opposed to actuating them with a polishing pad or fluid. The idea for such a process first originated in 1938 in the former Soviet Union[12]. It was later studied in other nations including Germany, Bulgaria, and the United States. Researchers in Japan and the United States have, in the past few decades, developed the process and realized commercial applications[13,14].

There are seemingly endless ways in which MAF can be applied; however, all setups posses similar components. All setups include one or more permanent magnets or electromagnets. They also include a ferromagnetic entity which either has abrasive properties itself or is in contact with a loose abrasive. MAF setups also have a means of achieving relative motion between the cutting edges of the abrasive particles and the surface intended for finishing.

There are many advantages to using MAF instead of conventional techniques, but there are also some applications in which MAF is the only suitable finishing technique. Perhaps the most prominent advantage of MAF is that it allows for finishing of surfaces inaccessible by conventional techniques. For example, in systems where clean gas is used, the piping and refills need to have smooth surfaces inside to prevent contamination by deposition of foreign substances. Shinmura and Yamaguchi used MAF to successfully polish the inside of a clean gas refill. The inside surface would normally be difficult if not impossible to access with a conventional polishing tool because it is not possible to insert the tool through the refill's small opening. Instead, the refill was partially filled with a "mixed-type" magnetic abrasive. This magnetic abrasive is a mixture of iron particles and abrasive particles. Permanent magnets outside of the refill were held stationary as the

refill was rotated. The magnetic abrasive also remained stationary inside the rotating refill as it was held by magnetic force. The relative motion between the abrasive particles and the rotating refill's inner surface and the pressure created by the magnetic force acting on the magnetic abrasive caused material removal which rendered a polished inner surface[15]. This is an example of how MAF can access previously inaccessible surfaces.

Another advantage of MAF is the non-rigid link between the actuating entity and the abrasive cutting edges. This occurrence is perhaps best illustrated by an example in which a standard wafer polishing machine setup is converted to employ MAF. In Figure 2-1, a normal wafer single-sided polishing setup is shown. The wafer to be polished sits atop a rotating table. Abrasive slurry is placed between the polishing pad and workpiece. A mechanical arm applies pressure to the polishing pad, maintaining it stationary as the table and workpiece rotate.

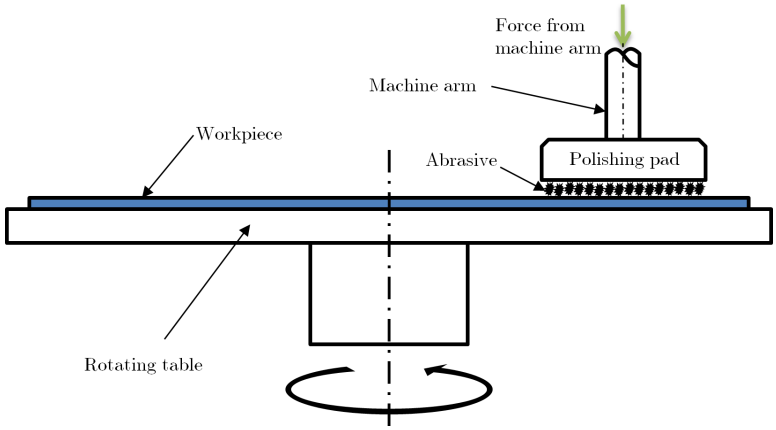

Figure 2-1. Schematic of a standard wafer polishing process.

The process in Figure 2-1 can be reconfigured to use MAF. The reconfigured process is shown in Figure 2-2; this is similar to the setup used by Yamaguchi *et al.* in 2009[16]. The polishing pad is assumed to be made of some ferromagnetic material, and instead of a machine arm pressing down on the pad, a permanent magnet resides beneath the rotating table. The magnetic force from the magnet attracts the polishing pad downwards, creating pressure on the abrasive particles and subsequently the workpiece. This configuration,

though similar to that of Figure 2-1, does not have a rigid link between the magnet and the abrasive particles. This means that any vibrations from the rotating plate, support structure of the magnet are not directly transmitted whereas in a standard polishing machine, any vibrations in the table or machine will be transmitted to the abrasive and subsequently to the workpiece. This non-rigid link allows for more precise surfaces and smoother finishes. This sort of improvement is required in the area of quartz or lens polishing, as any defects in the surface of the element tends to reduce the life of the part. The non-rigid link of MAF provides a gentler finishing process, reducing the amount of surface damage from the finishing process[17].

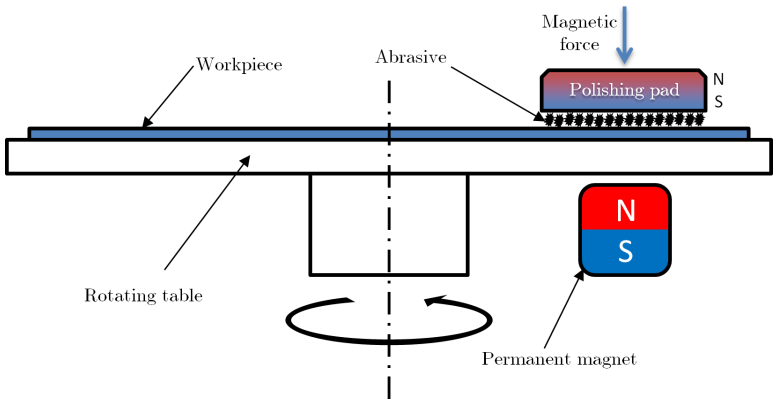

Figure 2-2. Schematic of a wafer polishing process modified to use MAF.

MAF is a high precision surface finishing process capable of finishing conventionally inaccessible surfaces. It is known as a form following and pressure copying process as the polishing tools tend to be flexible and can change in length in situ without affecting the finishing properties; this is known as the "flexible brush" created by the alignment of ferromagnetic particles along the magnetic lines of force in a magnetic field. The challenges of polishing of complex surfaces (contoured, textured) are sometimes easily overcome with MAF.

The force total force of a magnetic tool acting on a surface can be calculated using the following relationship:

$$\vec{F_m} = V\chi H \cdot \nabla H \tag{2–1}$$

where F_m is the magnetic force, V is the volume of magnetic particles, χ is the magnetic susceptibility, H is the magnetic field strength, and ∇H is the gradient of the magnetic field[18]. This equation is useful for determining the finishing pressure of the MAF process. However, it is not useful for determining the finishing force (cutting force of cutting edges of abrasive) because the arrangement of abrasive particles and magnetic particles is random. To clarify, the mechanism in MAF involves magnetic forces pulling the ferromagnetic particles towards the surface; material removal can only occur when abrasive particles are caught between the ferromagnetic particles and the workpiece surface. It is not possible to predict the amount of abrasive particles that are actually caught between the workpiece surface and ferromagnetic particles. It therefore is extremely difficult to predict the actual finishing force of an MAF process. This inability to predict finishing force is common to processes involving loose abrasives. However, like with most abrasive processes, the trends and effects of process parameters are understood mostly through empirical observations and these usually yield applicable knowledge.

There is some variety of ferromagnetic components used in MAF processes; these include: magnetic abrasives (ferrous particles with abrasive particles affixed to their surface), iron powder, magneto-rheological fluid (MRF), and magnetic fluid (MF). MRF is a mixture of small (5 μm diameter) iron particles and either a hydrocarbon or silicon based oil. MRF, when subjected to a magnetic field, becomes more viscous. This property allows it to be controlled in applications such as lens polishing where the finishing pressure needs precise control. MRF is used to polish surfaces to angstrom order roughness[19].

MF is a suspension of nanoscale magnetite particles (10 nm diameter) in water. There have been successful attempts at polishing with MF[20]. The force exerted by magnetic fluid is described by the following equation:

$$\vec{F_m} = \frac{1}{\mu_0} J_f V_f \nabla B \tag{2–2}$$

where F_m is the magnetic force, μ_0 is the magnetic permeability of vacuum, J_f is the magnetic polarization of the magnetic fluid, V_f is the volume of magnetic particles, ∇B is the gradient of the magnetic flux density[18]. Generally, the force of MF is less than that of MRF in the same magnetic field; this occurs because of the difference in volume of ferrous particles in the fluids. The larger particles of MRF are permeable to the magnetic field. Therefore, polishing with MF typically takes much more time and therefore MRF is preferred in most applications.

MAF has been shown to be scalable; it has been applied to normal sized workpieces as well as to micro-scale workpieces. The following sections will detail two processes which are relevant to this research, for they show the scalability of MAF and the use of an alternating magnetic field.

2.2 Static Magnetic Field Assisted Process

Yamaguchi *et al.* refined the application of MAF to the internal finishing of tubes. By rotating magnets around a tube and translating the rotating magnet assembly along the tube and adding a magnetic abrasive inside the tube, they were able to successfully polish the inner surface of nonferromagnetic bent tubes[21]. A similar process was scaled down and applied to capillary tubes; in this case, only the tube rotates, but the magnets still translate parallel to the tube's axis[22].

Figure 2-3 is a schematic of the processing principle for capillary tube polishing. As seen, the tube contains a small amount of magnetic abrasive. The tube rotates while the magnetic components reciprocate parallel to the tube's axis. The magnetic components consist of a permanent magnets linked by a piece of ferromagnetic material, in this case carbon steel, which acts as a magnetic yoke. The yoke tends to increase the magnetic field strength. Also attached to the permanent magnets are ferromagnetic devices called magnetic pole tips which concentrate the field at their narrow tips. Such geometry allows for more precise control of the abrasive and allows for the polishing of small diameter tubes.

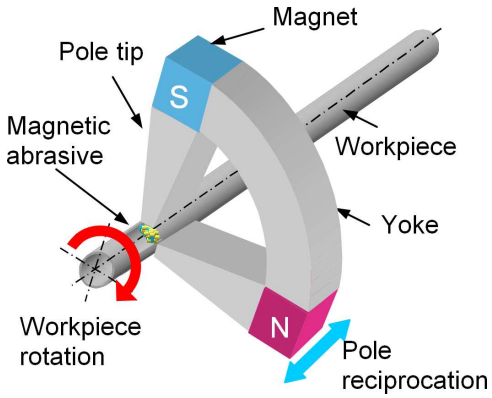

Figure 2-3. Schematic of processing principle for static magnetic field polishing process. [Courtesy of Hitomi Yamaguchi]

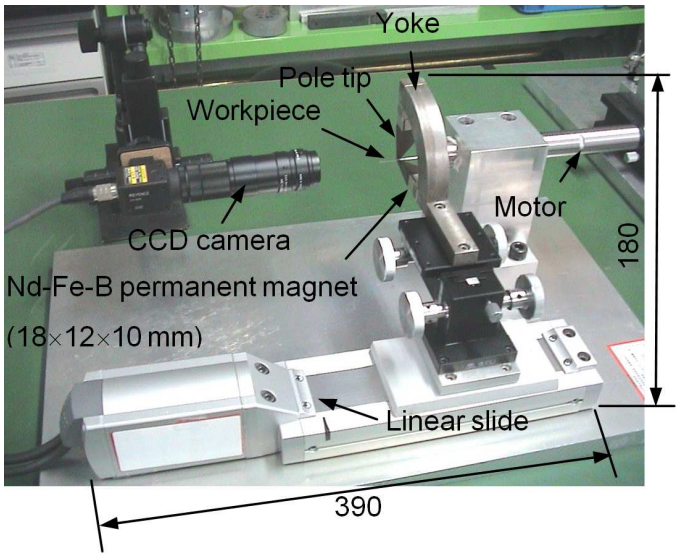

Figure 2-4. Photograph of static magnetic field assisted internal finishing equipment. [Courtesy of Hitomi Yamaguchi]

Figure 2-4 is a photograph of the capillary tube polishing machine setup. The motor and chuck assembly which hold the assembly are seen. Also the magnetic components are seen mounted on a two axis manual stage for proper positioning of the pole tips relative to the workpiece. The magnetic component/stage assembly is mounted onto a motorized linear stage which is then programmed to reciprocate the magnetic component/stage assembly parallel to the tube's axis[22].

Experiments conducted with this machine demonstrated that the inner surface of SS304 stainless steel tubes of 400 μm inner diameter having an initial surface roughness of

0.26 μm R_a was polished to 0.02 μm R_a[22]. This is an example of how MAF can be scaled to precisely polish surfaces inaccessible by conventional methods.

2.3 Alternating Magnetic Field Assisted Process

Though most applications of MAF are aimed at polishing a surface, it may also be applied as a surface texturing technique. In the following example, Yamaguchi *et al.* designed an MAF process to impart compressive stress to the inside of a pipe intended for critical high internal pressure conditions to increase the pipe's fatigue life. A conventional method for imparting compressive stresses on a surface is shot peening. However, shot peening cannot access the inside surface of a long pipe[23].

Figure 2-5 shows the processing principle for this process. As shown, there are two electromagnets facing each other; the coils are supplied with alternating current in a parallel configuration which creates an alternating magnetic field. A pipe is clamped on a chuck just beneath the electromagnetic pole tips. The magnetic tools used in this case are SS304 stainless steel pins, formed by cutting a wire into 2.5 and 5 mm segments. Although SS304 stainless steel is a paramagnetic alloy, cold working causes a change in microstructure, allowing the pins to become magnetized. The cold worked pins will naturally align themselves with the magnetic field direction. Therefore, if the field is alternating, the pins will continually realign themselves with the field direction. If the alternating frequency is high enough and if the pins were somehow suspended, they would rotate in a reciprocating fashion. The pins, however, are not suspended; instead, they are placed inside the tube. When an alternating field is applied to the working area, the pins begin to rotate and essentially jump off the inner tube surface. The results is a seemingly chaotic motion with the pins constantly striking the inner tube surface, thus creating regions of compressive stresses (dents).

Figure 2-6 shows a photograph of the machine. The opposing electromagnets are visible as is the workpiece. The function generator creates the alternating current for the electromagnets. Also the electromagnetic pole tips are shown with clearances labeled. This

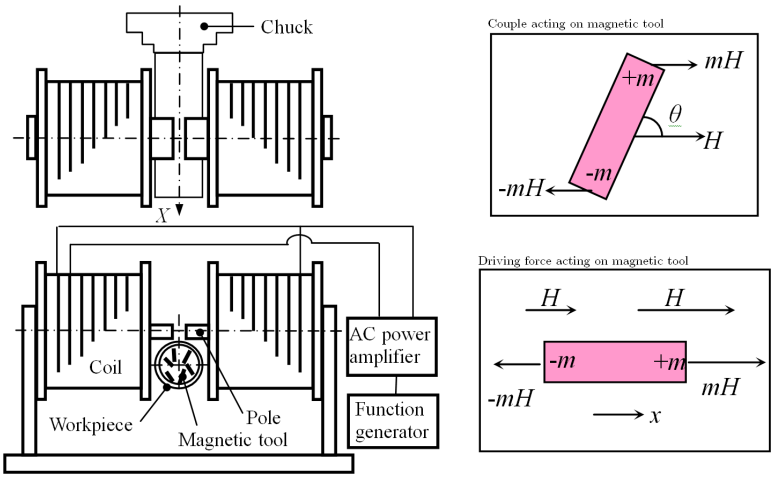

Figure 2-5. Schematic of processing principle for alternating magnetic field assisted machining process. [Courtesy of Hitomi Yamaguchi]

process was able to successfully raise the hardness and compressive residual stresses of the inner tube surface. This is an example of an alternating MAF process for a surface texturing application.

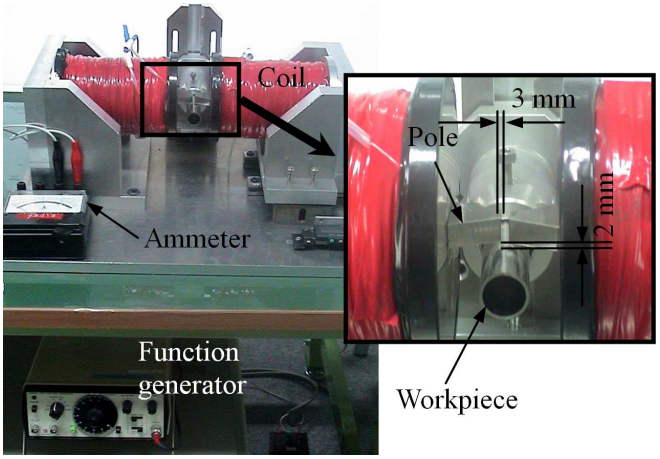

Figure 2-6. Photograph of alternating magnetic field assisted machining equipment. [Courtesy of Hitomi Yamaguchi]

CHAPTER 3
DEVELOPMENT OF PROCESS PRINCIPLE AND POLISHING MACHINE

3.1 Micro-Pore X-Ray Mirrors

Figure 3-1 shows a photograph of an x-ray mirror made by JAXA. This silicon micro-pore x-ray mirror is 100 mm in diameter and only 300 μm thick. The slits are 5 - 20 μm wide and vary in arc length from less than 1 mm to nearly 10 mm and extend through the thickness of the silicon substrate; the slits were created by DRIE on a commercially purchased high quality silicon wafer.

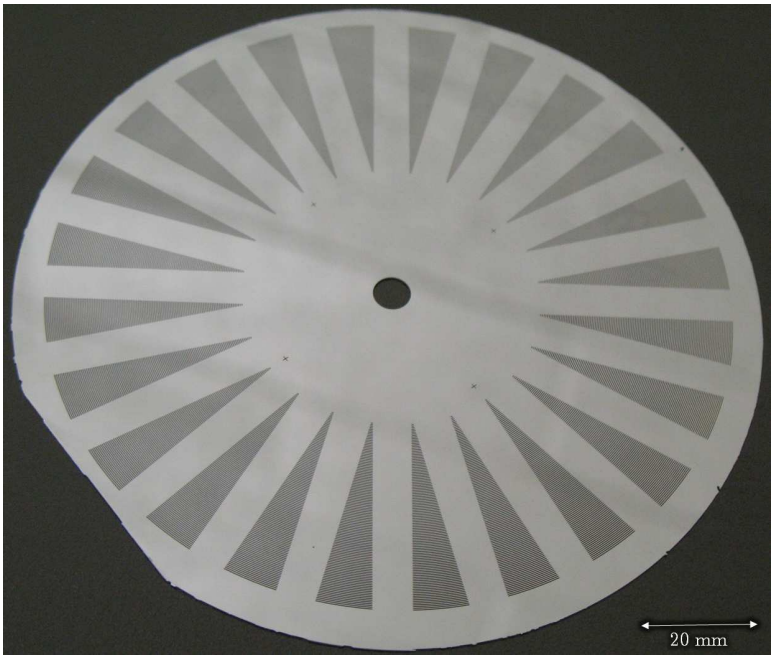

Figure 3-1. Photograph of a silicon single stage Wolter type I optic fabricated by DRIE.

The mirrors function is briefly explained in Figure 3-2. The mirror in top-view represents the mirror from Figure 3-1. As can be seen from the cross-sectional view, the slits are to increase in width as the radius increases. The lowermost graphic in Figure 3-2 shows the mirror deformed so that the micro-pore sidewalls are angled such that incident x-rays are spectrally reflected and focused onto a point. JAXA is in collaboration with another group at Tohoku University in Japan who has been able to plastically deform

silicon wafers[24]. The group at Tohoku University is currently able to deform the mirror in Figure 3-1, giving it a spherical shape having a radius of approximately 1000 mm.

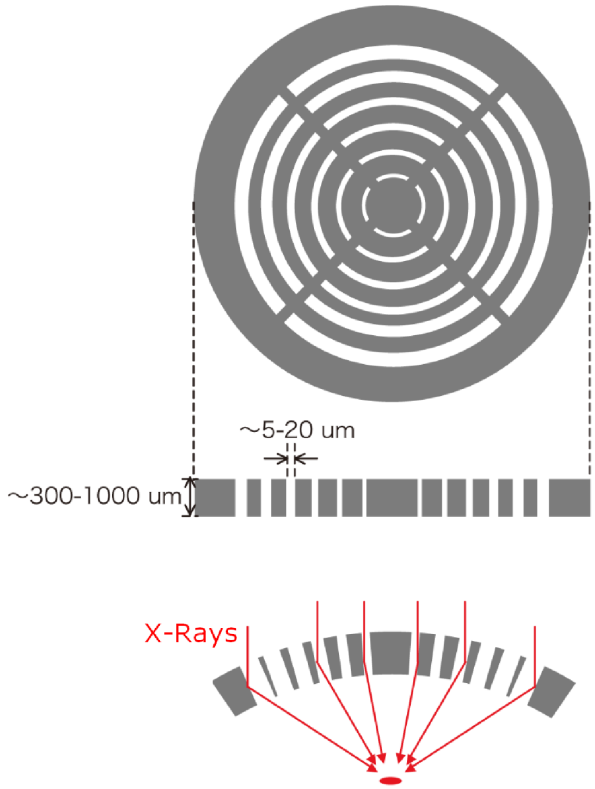

Figure 3-2. Schematic of the function of a micro-pore x-ray mirror.

Although JAXA can create the mirror and Tohoku University can deform the mirror to the desired spherical shape, the micro-pore sidewall roughness is too high to attain spectral reflection of incident x-rays. This is not an unexpected result as typical roughness for the sidewalls of features created by DRIE is around 30 nm *rms*[9]. Therefore, the mirror is not functional. The sidewalls need to be polished; this is the University of Florida's task.

To attempt to solve the sidewall roughness dilemma, JAXA provided miniature workpieces with micro-pores etched on them of similar geometry to the full-size micro-pore x-ray mirror. These miniature workpieces are called "mirror chips" and a photograph of a silicon mirror chip is shown Figure 3-3. The micro-pore width is constant on these mirror

chips. The yellow tabs on each corner are simply bits of polymide tape to affix the mirror chip during shipping.

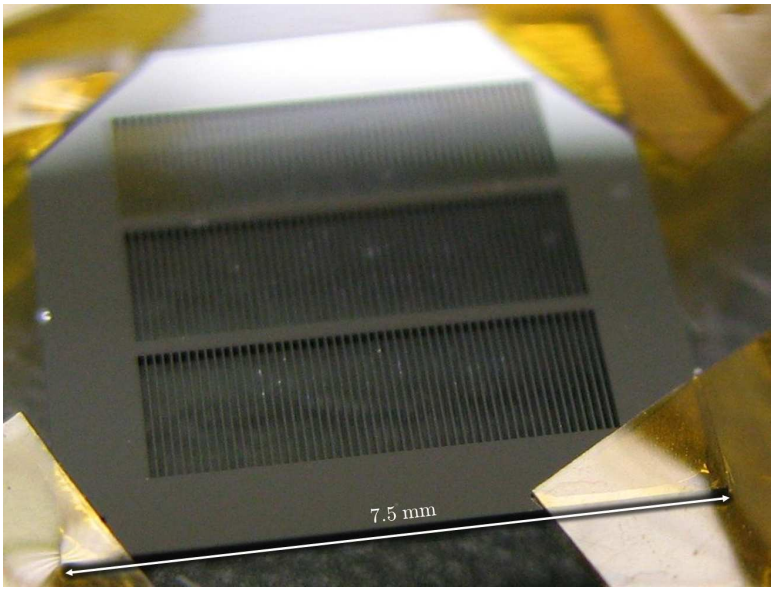

Figure 3-3. Photograph of a silicon mirror chip fabricated by DRIE.

JAXA is collaborating with Fumiki Kato of Ritsumeikan University in Japan to fabricate nickel mirror chips by x-ray LIGA. Mr. Kato was able to fabricate a limited number of nickel mirror chips. A photograph of a nickel mirror chip fabricated by LIGA can be seen in Figure 3-4. Although the sidewall surface roughness of nickel structures made by LIGA is better (10 nm *rms*[11]) than that of silicon mirror chips fabricated by DRIE, the sidewalls are still too rough to attain spectral reflection. Nickel mirrors chips also need to be polished. In Figure 3-5, the PMMA mold from the LIGA process is shown; this is before the mold is sputtered with gold. To clarify, the mold seen in Figure 3-5 is the at step 3 in Figure 1-11.

Figure 3-6 shows a side by side comparison between the full-size x-ray mirror and a silicon mirror chip. Once testing is complete on mirror chips and a suitable micro-pore sidewall surface roughness is achieved, attempts at polishing a full-size x-ray mirror may begin.

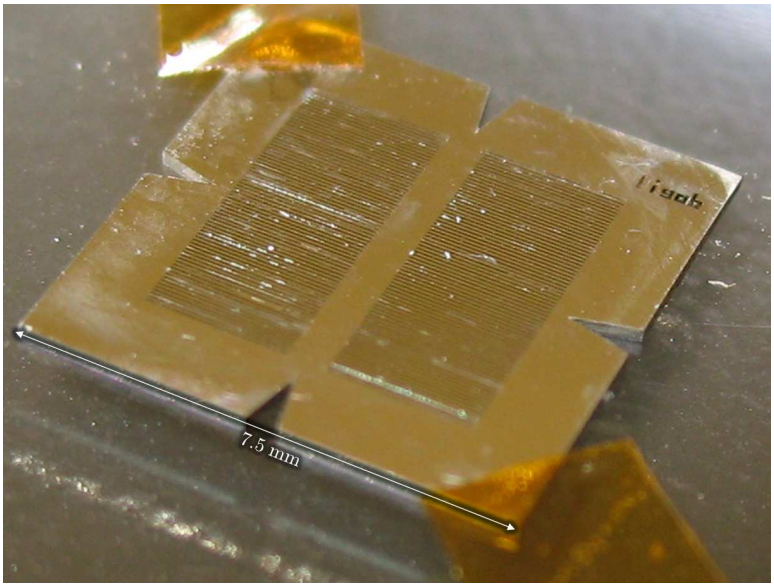

Figure 3-4. Photograph of a nickel mirror chip fabricated by LIGA.

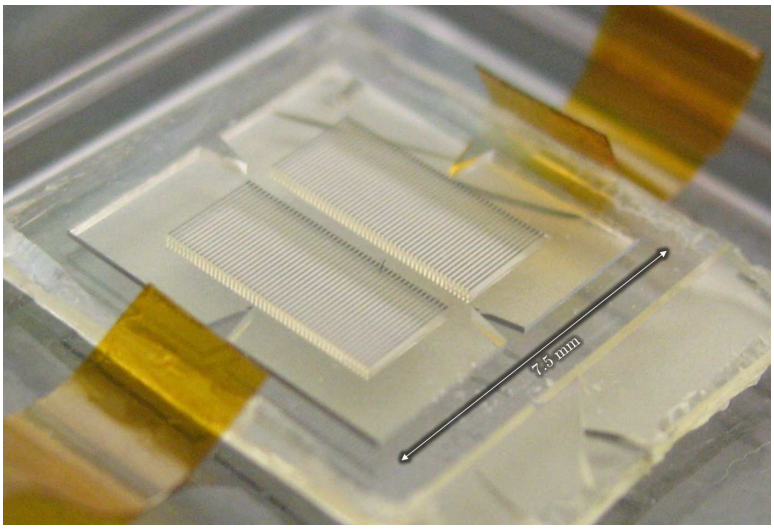

Figure 3-5. Photograph of a LIGA mold used to create a nickel mirror chip. This is an example of the mold described in step 2 of Figure 1-11.

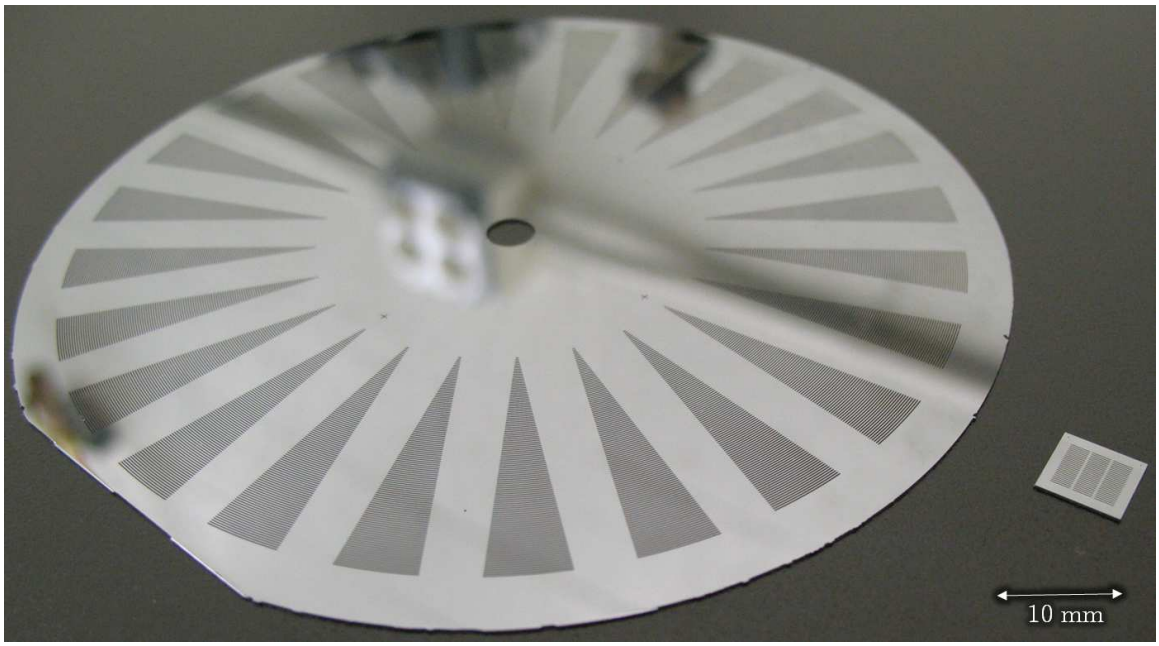

Figure 3-6. Size comparison between a full optic and a mirror chip. Both structures shown are made of silicon and fabricated by DRIE.

3.2 Processing Principle for Micro-Pore X-Ray Mirror Polishing

The challenge was to polish the micro-pore sidewalls the mirror chips to a surface roughness of less than 1 nm *rms*. There is no conventional polishing process capable of accessing such surfaces. When complex surfaces or part features in industry need polishing, finishing, or deburring, the operations are done by hand or robots; however, these features are far too small to polish by hand or even by precise machines. One could suggest the use of ultra-precision machine tools combined with a rotating polishing tool. Ultra-precision machine tools are sometimes able to move in nanometer increments. However, a rotating tool would have run-out that could damage the sidewall surface. There exists a non-traditional polishing technology called abrasive flow machining (AFM) which involves abrasive particles mixed with some fluidic media which is forced through and around part features leaving them polished, rounded, and deburred. AFM can polish features of small diameters such as micro-pores; however, the pressure differentials required to force abrasive media through the micro-pores would likely break the thin wafer.

Micro-pores are small and inaccessible. There were no technologies previously available to polish such features. MAF has been shown to be scalable and be able to access previously inaccessible surfaces. It was therefore thought suitable for attempting to polish the micro-pore sidewalls of mirror chips.

Micro-pores, with regard to the micro-pore x-ray mirror, range in width from 5 to 20 μm. The lower limit of 5 μm rules out the use of any magnetic abrasive particles, iron powders or magneto-rheological fluid (MRF) as a ferromagnetic component of the MAF process as they range in size from 5 μm to hundreds of microns. The only ferromagnetic component fine enough to work inside micro-pores is magnetic fluid (MF). The small slit width also limits the size of abrasive that can be used; fortunately though, there are commercially available abrasives having a mean particle diameter as small as 50 nm.

Choices for a magnetic abrasive combination of materials were rather limited. MF is commercially available and is commonly based in either kerosene or water. Water based MF was chosen for this application because it rinses easily and without residue; water based MF is more environmentally friendly than kerosene based MF. Through trial and error, it was found that MF does not mix easily with commercial powder abrasives because agglomeration of particles occurs. It also does not mix well with commercial abrasive slurries as it tends to form a precipitate. It was found that it only mixes well with some water based abrasive slurries (depending on the manufacture's specific surfactants) and with universal abrasive slurries which are able to homogeneously mix with both water and oil based fluids.

The basic concept of a processing principle involved using a mixture of MF and abrasive slurry as a magnetic abrasive. This mixture would be placed inside the slits and a magnetic field would be used to force the mixture on the micro-pore sidewalls to polish them. To place the magnetic abrasive fluid inside the micro-pore slits, the mirror was to be submerged in the magnetic abrasive fluid. In order to polish the micro-pore sidewalls, there had to be relative motion between the abrasive cutting edges and the micro-pore

sidewall surface. The idea to use an alternating magnetic field then came about. It was thought that the magnetic abrasive fluid could reciprocate back and forth across the micro-pore sidewall surface under an alternating magnetic field.

The processing principle shown in Figure 3-7 was conceived. In an alternating magnetic field, the strength and direction are transient. To represent the process schematically, two states were chosen: State 1 and State 2. These states correspond to the points in time where the magnetic field strength is at its maximum in both directions. The alternating magnetic field is created by two cylindrical electromagnets facing each other coaxially, as in the machine described in section 2.2. The mirror chip is positioned such that its large flat faces are perpendicular to the electromagnet's axis. In this arrangement, the fluid should essentially move from one electromagnet to the other repeatedly, thus polishing the micro-pore sidewalls.

3.3 Design Concept and Specifications of Polishing Machine

Once a processing principle was established, a machine needed to be built. Based on previous designs of machines similar in function to what was required for this polishing process, specifications were defined. A machine would have to have features such as

- two inward facing electromagnets with interchangeable magnetic pole tips and an adjustable gap between them,
- the ability to create a controllable alternating magnetic field given alternating current (AC),
- and a multi-purpose workpiece holding platform able to precisely position the workpiece.

These requirements are broad; a more specific description is offered the Table 3-1. In the next section, the actual machine design will be presented.

3.4 Polishing Machine

3.4.1 Design and Build

A computer aided design (CAD) model of the polishing machine was created and is shown in Figure 3-8. The design features interchangeable magnetic pole tips and a

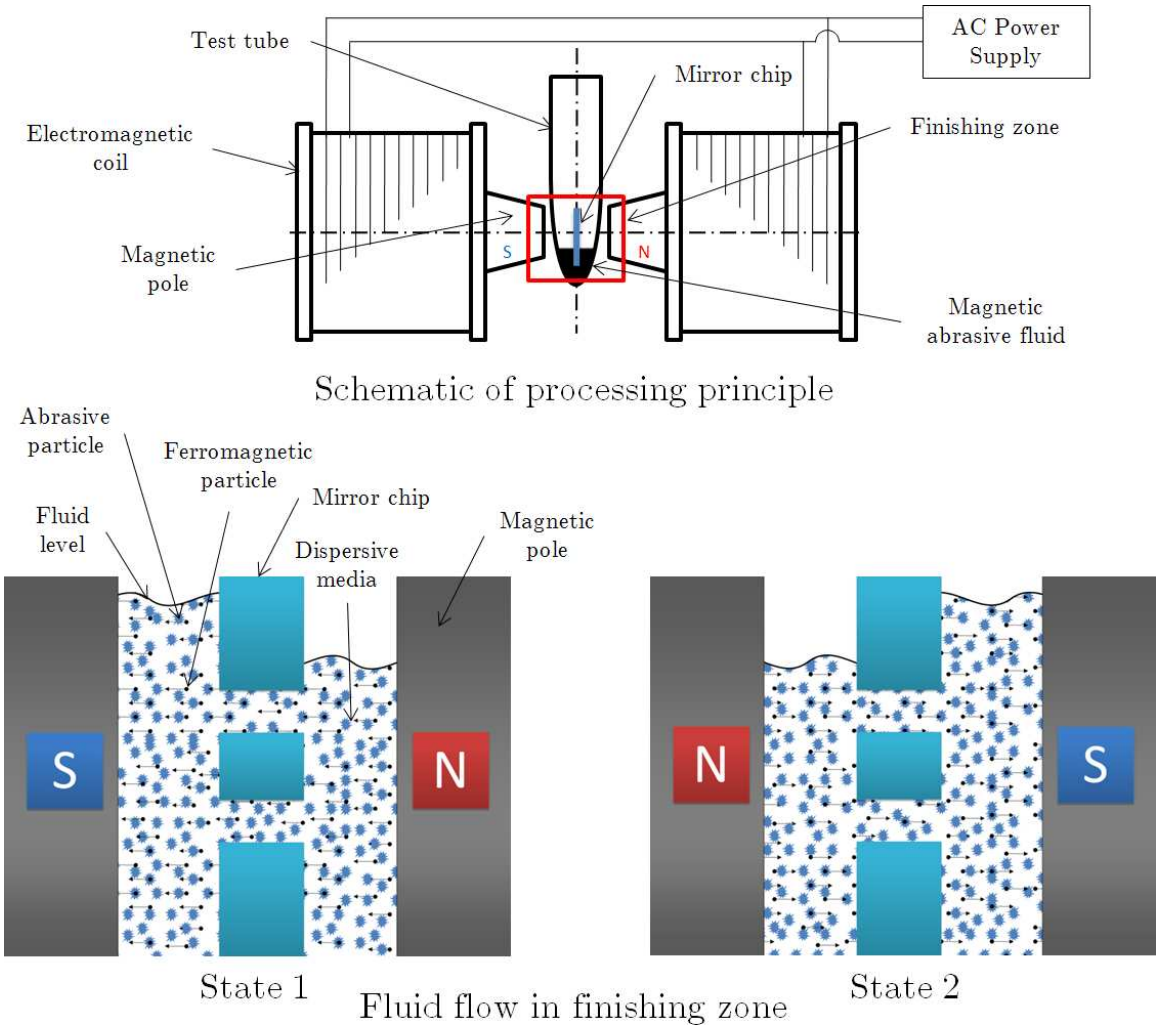

Figure 3-7. Two-dimensional schematic of processing principle.

magnetic yoke, delineated in Figure 3-9. Both electromagnets are mounted on linear bearings and are actuated by a double threaded lead screw (half right hand thread, half left hand thread). This stage setup allows the electromagnets to move symmetrically, creating space on both sides of the work area for easier access. A digital linear scale is attached to both electromagnet stages and reads the inter-pole gap. The three axis manual stage is available for workpiece jig mounting. Adjustable machine feet allow the machine to be leveled.

Figure 3-9 shows the magnetic components of the machine outlined in red. The pole tips are designed to increase the strength of the magnetic field at the inter-pole gap. The

Table 3-1. Machine specifications.

Feature	Property	Description
Electromagnets	Interchangeable magnetic pole tips	Attached using a threaded stud.
	Adjustable inter-pole gap	Electromagnets mounted on linear bearings and are position by a leadscrew.
Magnetic field	Alternating	An AC power supply connected to electromagnet terminals.
	Controllable	A flexible circuit able to change the circuit from parallel to series. AC power supply can vary voltage and frequency.
Workpiece holder	Precise and adaptable	A three axis-manual positioning stage with 50mm travel in each axis with coarse and fine position adjustment allows for many mounting options.

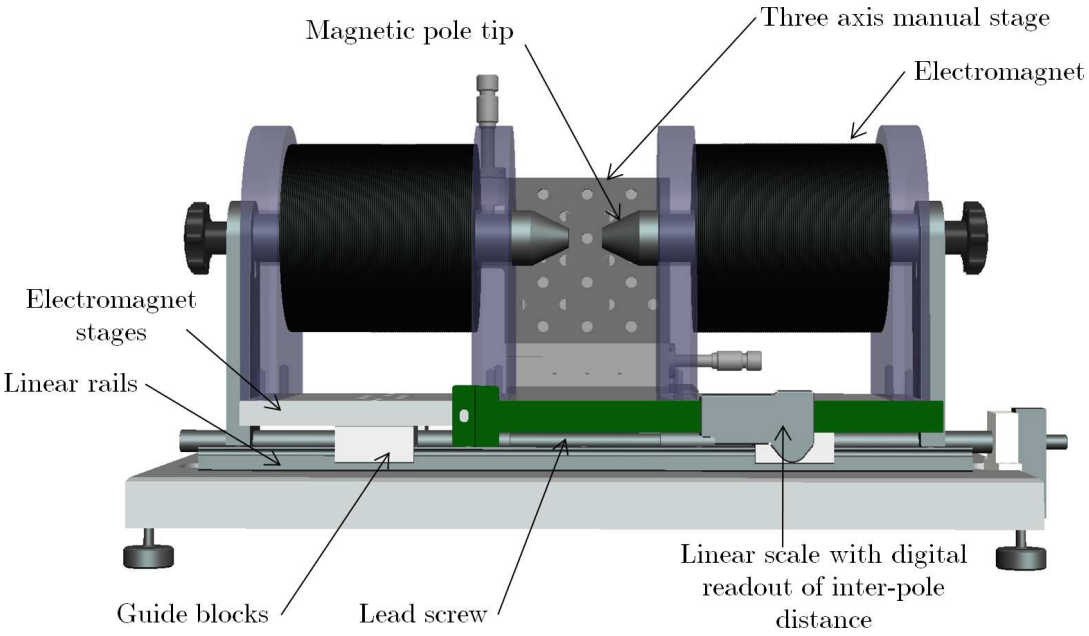

Figure 3-8. CAD design of polishing machine.

magnetic yoke is composed of three parts: two yoke sides and a yoke bottom. This yoke is intended to increase the strength of the magnetic field by using its magnetic permeability to carry the magnetic flux from one electromagnet end to the other[18].

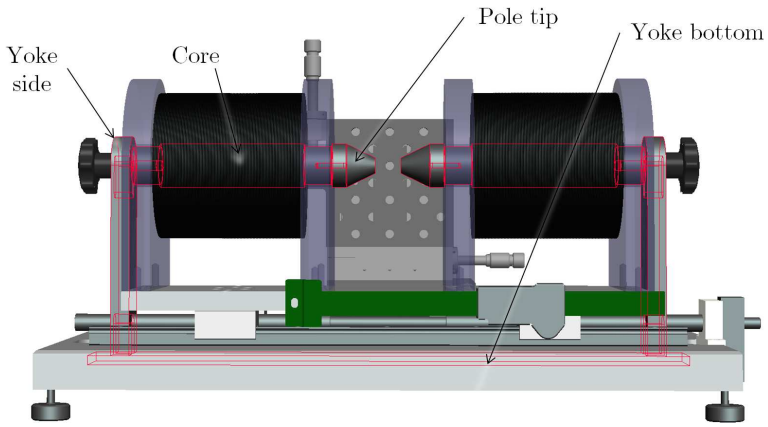

Figure 3-9. Magnetic circuit is shown in this CAD model. The magnetic components (pole-tips, coil cores, and yoke) are delineated in red.

Figure 3-10 is a photograph of the completed machine. Figure 3-11 shows the experimental setup which includes the machine and power supply. The power supply is a Kikusui model PCR 1000LA. This power supply is actually a high current signal generator able to supply a variety of waveforms at several amperes. The frequency range for AC current is 0 to 1000 Hz. It is therefore suitable for an experimental electromagnet setup such as the one in Figure 3-10 because it allows for experimentation with different waveforms to force different dynamic responses from the magnetic abrasive fluid.

3.4.2 Dynamic Motion of Ferrous Slurry

Initial polishing attempts on mirror chips made some problems with the initial design and the lack of a solid experimental procedure became apparent. None of the initial polishing attempts yielded any improvement in the mirror chips' sidewall surface roughness. In fact, there was no definite indication of any material removal from any of the analysis techniques used which included weight measurements with a microbalance, optical microscopy, and surface profiling with a scanning white light interferometer. After

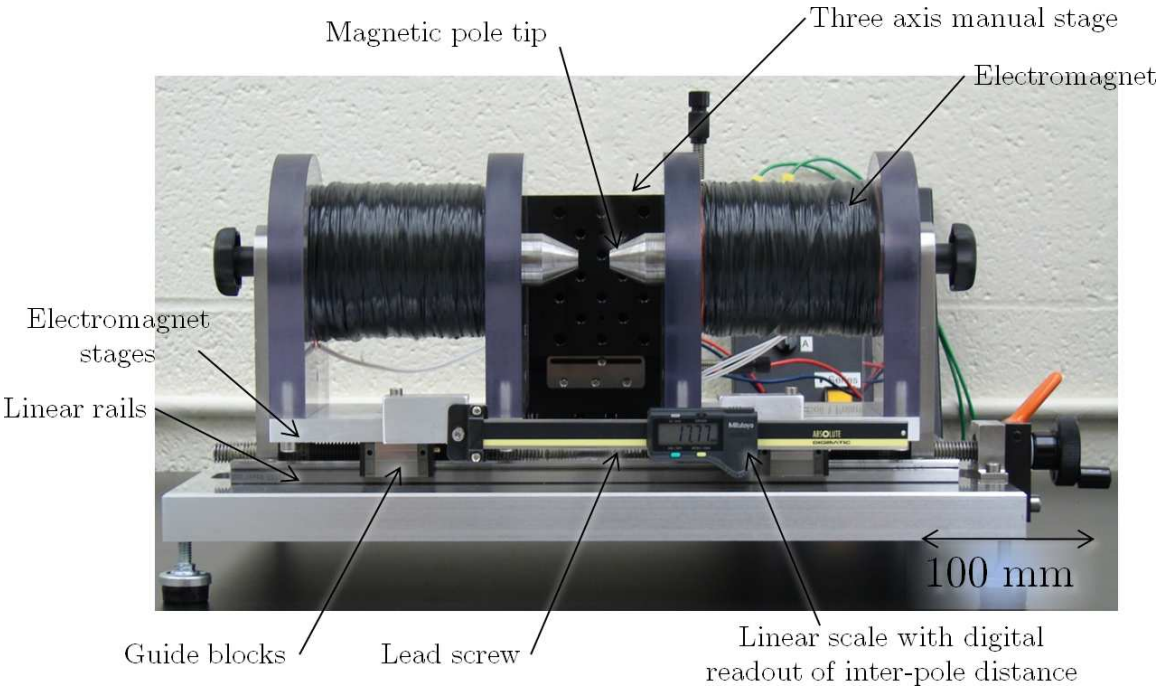

Figure 3-10. Photograph of completed polishing machine.

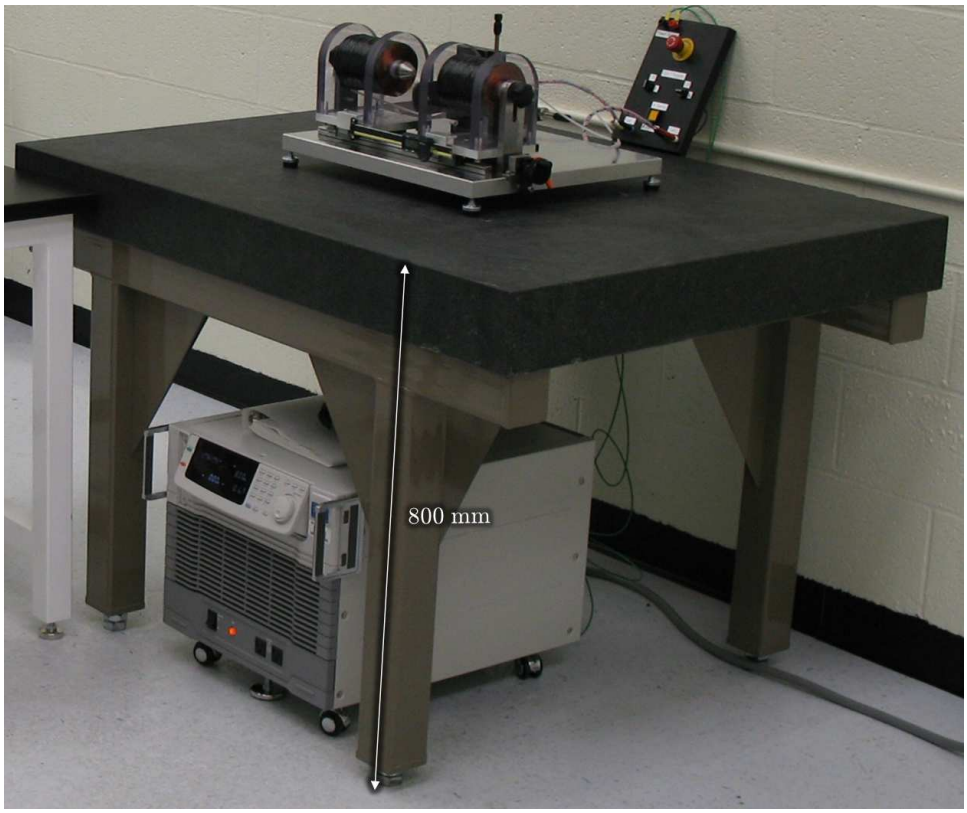

Figure 3-11. Workstation setup including completed machine, power supply, and surface plate.

a thorough examination of the polishing machine's design, it was determined that the originally envisioned processing principle was not being realized by the machine.

The problem laid in the original circuit design shown in Figure 3-12. The two electromagnets (coils) are supplied current in parallel. It is clear from examining the current flow through each electromagnet that each coil receives the same waveform. When the current waveform is at its crest, both electromagnets are generating magnetic fields at full strength and in a direction determined by their wiring. The electromagnets are both at full strength at the trough of the supplied wave but their magnetic field directions are switched. In other words, the electromagnets are behaving symmetrically.

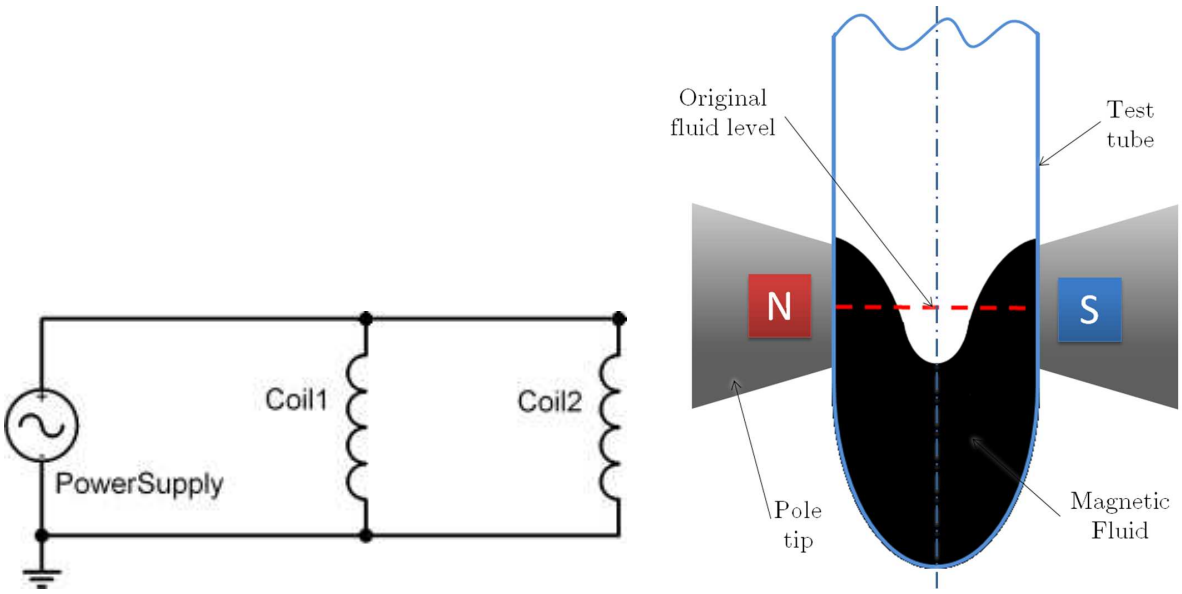

A Original circuit

B Schematic of fluid behavior

Figure 3-12. Original electric circuit and a two-dimensional schematic of the corresponding fluid behavior.

The effect that this symmetrical electromagnet behavior on the fluid behavior is described in Figure 3-12. The fluid takes on a symmetrical behavior. As seen, a portion of fluid is placed inside a plastic test tube and the tube is positioned between the machine's pole tips. Figure 3-13 is a still frame from a video taken of the dynamic fluid motion. The

fluid is simply pulled apart, with equal portions attracted to both coils. This symmetric behavior does not accomplish the processing principle presented in Figure 3-7.

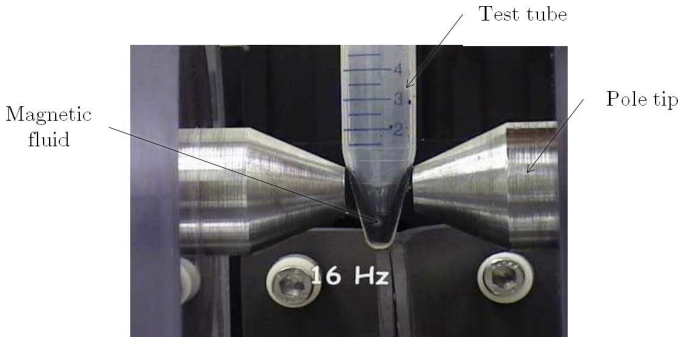

Figure 3-13. Fluid motion using original circuit. [Conditions: MF 1mL, 1 A, 16 Hz, Pole-pole distance 12 mm]

An alternating magnetic field is not necessary to achieve this fluid behavior; supplying the coils with sinusoidal current ranging from no current to maximum current would accomplish the same macroscopic fluid behavior. It is known that MF does not exhibit any hysteresis or coercive force[18]. Therefore, the alternation of a magnetic field has no special effect on the behavior of MF.

A modification was required to make the fluid behave as intended. A change to the circuit was made; this modified circuit is shown in Figure 3-14. A set of diodes were included in the circuit to modify the current flow to both electromagnets. Instead of each coil receiving a full-wave, each coil now receives an opposite half-wave. A plot of this behavior is shown in Figure 3-14. It was thought that this electric circuit would realize the processing principle of Figure 3-7, as only one coil is active at a time, allowing for State 1 and State 2 to exist. A schematic of the fluid behavior observed is shown in Figure 3-15. Instead of symmetrical motion, the fluid now is attracted to only one side at a time.

A photograph of State 1 and State 2 of the fluid motion is shown in Figure 3-16. The fluid does not exhibit symmetrical motion. A few preliminary polishing trials using the modified circuit did indeed cause significant material removal as changes in surface roughness were observed.

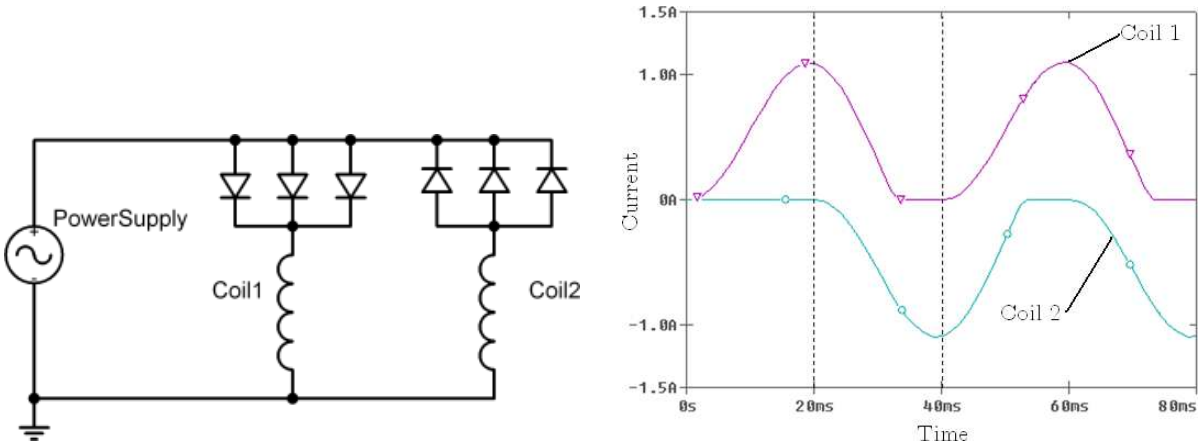

A Modified circuit

B Current behavior of modified circuit

Figure 3-14. Modified circuit and current plot.

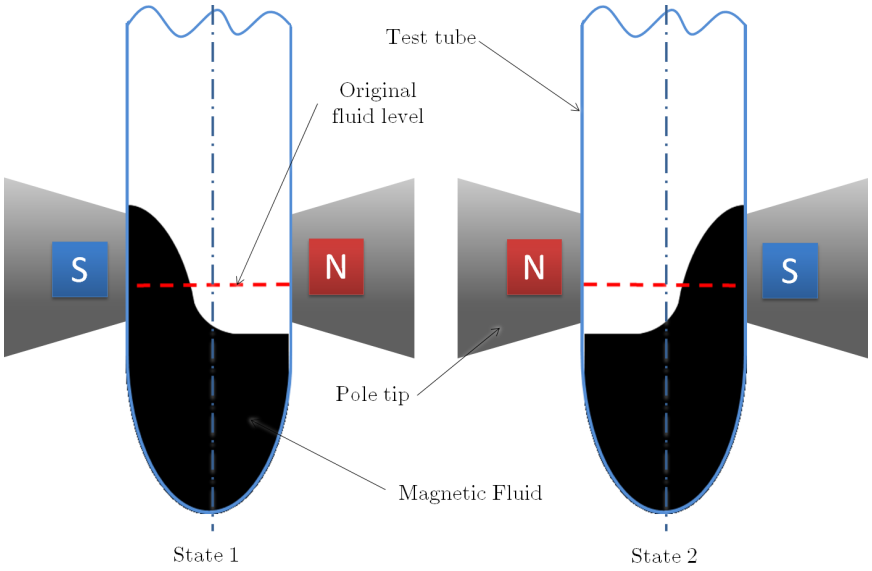

Figure 3-15. Two-dimensional schematic of fluid behavior with modified circuit design.

This modified circuit changes the function of the machine. Instead of creating a purely alternating field, the machine now creates an alternating and switching field, where the term "switching" implies that, at certain points during the machine's operation, only one electromagnet is active. Since the magnetic field generated by the machine is transient, it is best to represent its behavior using the previously defined states 1 and 2 as shown in Figure 3-17. In State 1, the left coil is active and the arrows indicate of the flow of magnetic flux. In State 2, only the right coil is active. It is important to note that State

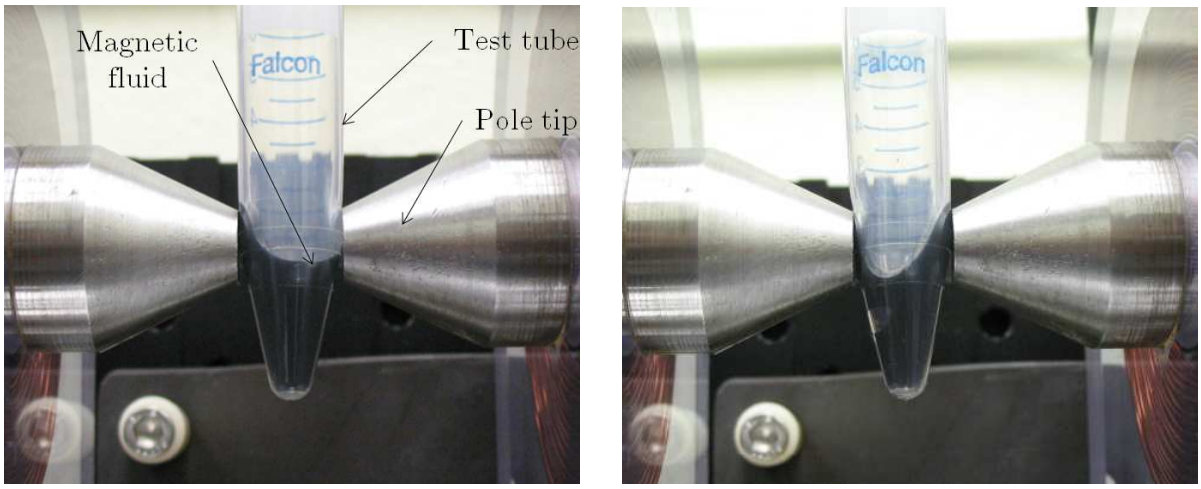

A State 1 B State 2

Figure 3-16. Fluid motion using modified circuit. [Conditions: MF 1 mL, 1.4 A, 2 Hz, Pole-pole distance 15 mm]

1 and State 2 correspond to the current states at 20 ms and 40 ms of the simulation in Figure 3-14.

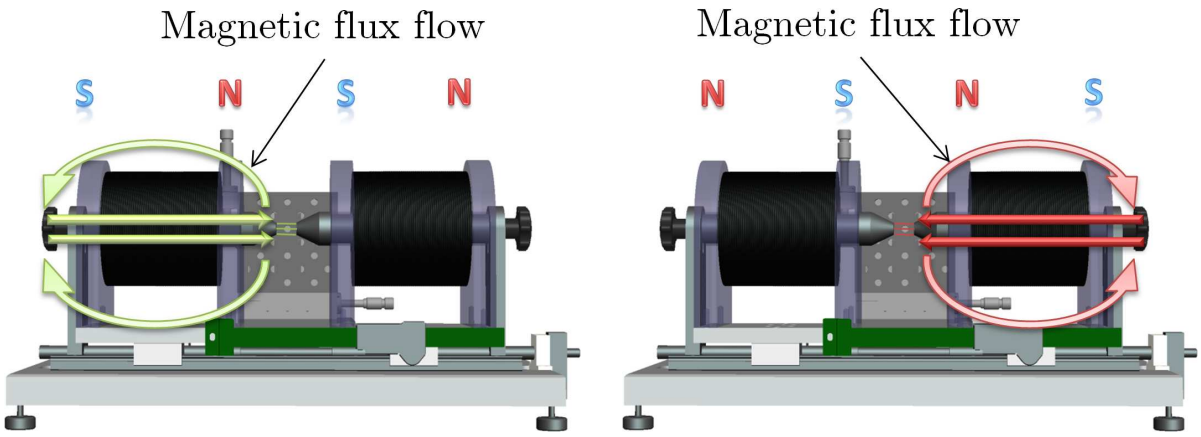

A Magnetic field at 20 ms of simulation B Magnetic field at 40 ms of simulation

Figure 3-17. Schematic of transient states of magnetic field during operation.

CHAPTER 4
POLISHING CHARACTERISTICS

4.1 Surface Roughness Analysis

In the field of surface engineering, surfaces are characterized by a variety of methods. The analyses performed in this research were done with an optical profiler (Zygo NewView 7200) which uses scanning white light interferometry to measure a surface. The data created by the optical profiler is simply a point field, where each data point has X, Y, and Z coordinates. Using Zygo's MetroPro software, the data may be visualized in a variety of ways and also many analysis methods are available.

The profiler, using the available magnification, is able to image an area as small as 176 × 133 μm with 640 × 480 lateral resolution. The data is typically analyzed as a map (area) of surface. From this map, surface roughness values such as the roughness average (Ra), root-mean-squared roughness (rms), and peak to valley distance (PV) are calculated. Figure 4-1 shows a schematic of a profile of a single line of data points with examples of roughness values. The Ra value is a simple average of the distance of all

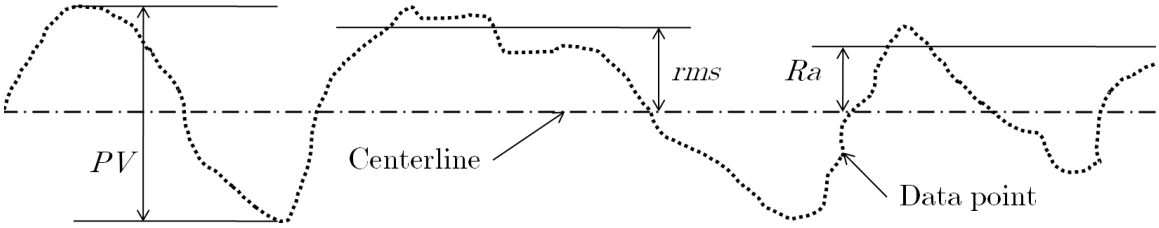

Figure 4-1. Schematic of a surface profile.

points from the centerline. The Ra value is calculated as follows,

$$Ra = \frac{y_1 + y_2 + y_3 \cdots + y_N}{N} \tag{4–1}$$

where y_x are the height values of a measured data point, and N is the number of data points[25]. The rms roughness is the root-mean-square of the distance of all data points

from the centerline. The *rms* value is calculated as follows,

$$rms = \sqrt{\frac{y_1^2 + y_2^2 + y_3^2 \cdots + y_N^2}{N}} \tag{4–2}$$

where y_x are the height values of a measured data point, and N is the number of data points[25]. Though both of these values are similar, their use is determined by the specific application. For example, if a surface is being prepared for anodizing, only its *Ra* value may need specification. However, if the surface of an optical device needs to have minimal diffusion of the reflected light, the *rms* value should be specified, as it tends to give more weight to larger deviations in the surface profile.

The PV value is simply the difference between the highest point to the lowest point in the map or profile. This factor is used to describe the quality of the surface. For example, if a polishing process leaves a generally smooth surface but suffers from agglomeration of abrasive particles causing occasional deep scratches, then the surface will have low *Ra* and *rms* values, but it will have a high PV value.

Any deviations on a real surface from a perfectly flat surface are referred to as surface errors. Surface errors are often times periodic in nature and their wavelength can be measured. Surface errors are typically classified into two major wavelength groups, waviness and roughness. Figure 4-2 shows the relationship between these two classifications; the boundaries defining the difference between waviness and roughness are determined by the intended application of the surface.

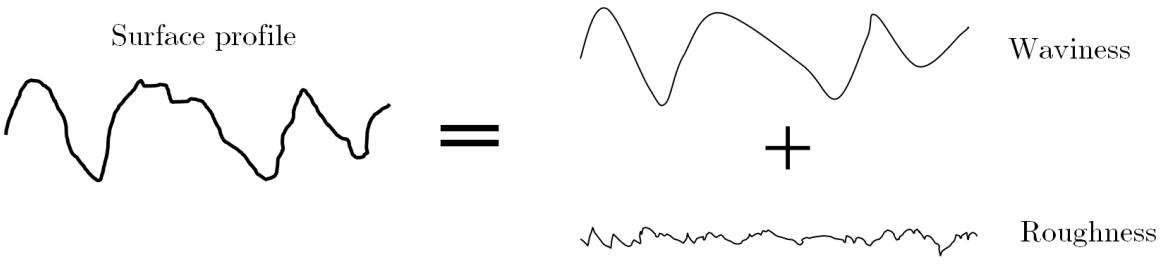

Figure 4-2. Schematic of a surface profile broken down into waviness and roughness.

To find the value of the roughness of a surface, the waviness is often removed by filtering the measured data. Many filters exist which are useful for surface roughness analysis such as Gaussian spline and moving average types. In this research, two filters are used as the surface of mirror chip sidewalls tends to have large wavelength errors.

4.2 Experimental Procedure

After a few initial polishing trials, a procedure for running polishing trials on mirror chips was established. The first challenge was finding a way to hold the mirror chip steady during the polishing trial. This work-holding problem was solved by fabricating a specialized mirror-chip holder which not only is able to hold a single mirror chip also fits inside a test tube. The holder consists of two major parts, the mirror chip clamp and the handle as shown in Figure 4-3. The mirror chip clamp is two thin (0.5 mm) plates with an opening milled out to expose the mirror chip's micro-pores. One of these plates has a square inset area to account for the mirror chip's thickness when clamped between the two plates. An M3 threaded 316L (paramagnetic) stainless steel bolt clamps the two plates together at one end. The handle is simply an aluminum rectangular prism with a deep slot going through one of its ends. The mirror chip clamp slides inside this slot and an M4 threaded 316L stainless steel bolt clamps the other end of the mirror chip clamp in the handle's slot.

Once the mirror chip is clamped in the mirror chip clamp and that assembly is clamped in the handle, the wafer and holder assembly is placed inside a test tube. The test tube is then placed between the polishing machine's pole tips. To run an actual test, the tube is filled with the magnetic abrasive fluid before the mirror chip/holder assembly is placed inside. It is important to note that the level of the magnetic abrasive fluid relative to the mid-height of the mirror chip should be coincident before the alternating and switching magnetic field is applied.

Once the mirror chip is both mounted on the machine and partially submerged in magnetic abrasive fluid, the power supply is powered on, activating the magnetic field.

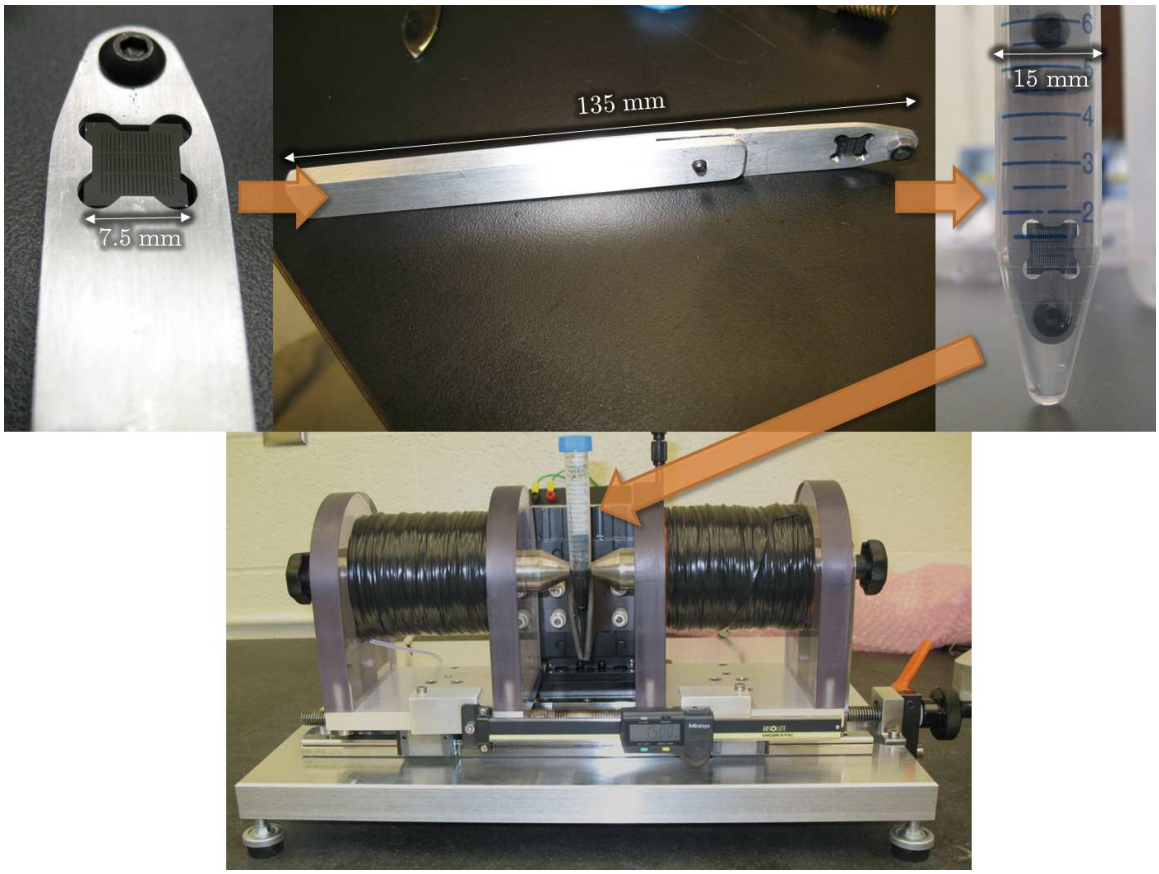

Figure 4-3. Photograph of experimental setup with a mirror chip mounted.

The user will examine the fluid agitation visually and determine if the amount of agitation is sufficient, as the current assumption is that maximum fluid motion is desired for the most efficient finishing. Typically, if more agitation is needed, the wafer holder assembly is pulled out of the test tube a small distance (1 - 2 mm). If less agitation is needed, the wafer holder assembly is positioned deeper inside the test tube. The wafer assembly fits inside the test tube with a slight interference, it is this fit that allows the wafer holder assembly to be positioned as seen fit by the user.

Regarding the magnetic abrasive fluid, it is produced by first placing 1 mL of MF inside the test tube. Next, 1 mL of abrasive slurry is placed inside the tube as well. The user will homogenize the mixture by briskly waving a strong permanent magnet outside of the tube; this causes the fluids to mix well. In the following section a series of experiments done on silicon mirror chips is presented. It should be known that every polishing trial

presented in this document used 2 mL of magnetic abrasive fluid, and after each polishing trial, the mirror chips were removed from the tube and holder for cleaning. The cleaning process involved placing the mirror chip in an ultrasonic cleaner for 5 minutes in a solution of water and a mild detergent. The mirror chip was then placed in an ultrasonic ethanol bath for another 5 minutes.

4.3 DRIE-Fabricated Mirrors

4.3.1 Unpolished State

JAXA provided about 20 mirror chips for testing of the polishing process. Each wafer had different micro-pore dimensions. There are three basic dimensions used to define the shape of the micro-pores on a mirror chip; they are micro-pore width, micro-pore spacing, and micro-pore radius of curvature. The micro-pore width is simply the slit width. Micro-pore spacing is the distance between any two micro-pores on a mirror chip in within a column of slits. The micro-pores have a slight radius (50 to 250 mm) so that they more closely represent the slits on the full-size x-ray mirror.

Figure 4-4 shows a micrograph of an unpolished DRIE-fabricated mirror chip micro-pore sidewall. As seen in the figure, the surface's texture varies in the etching direction and in the direction perpendicular to the etching direction. Due to this non-uniform surface texture, a single measurement of the entire surface would not accurately represent the roughness of the sidewall. Instead, only an 80 μm^2 area was used for roughness analysis. This area is placed in the approximate center of the sidewall surface where the texture tends be more uniform.

Figure 4-5 shows an oblique plot from a measurement taken of an unpolished mirror chip micro-pore sidewall with an optical profiler. Roughness values tend to range from 10 nm *rms* to 15 nm *rms* depending on where the measurement is taken. This measurement's peak to valley (PV) reading was 100 nm. The wafers supplied were sorted into groups first by micro-pore width, then by micro-pore spacing, and finally by radius. Having grouped the wafers, a testing plan was created to examine the effects of various process parameters.

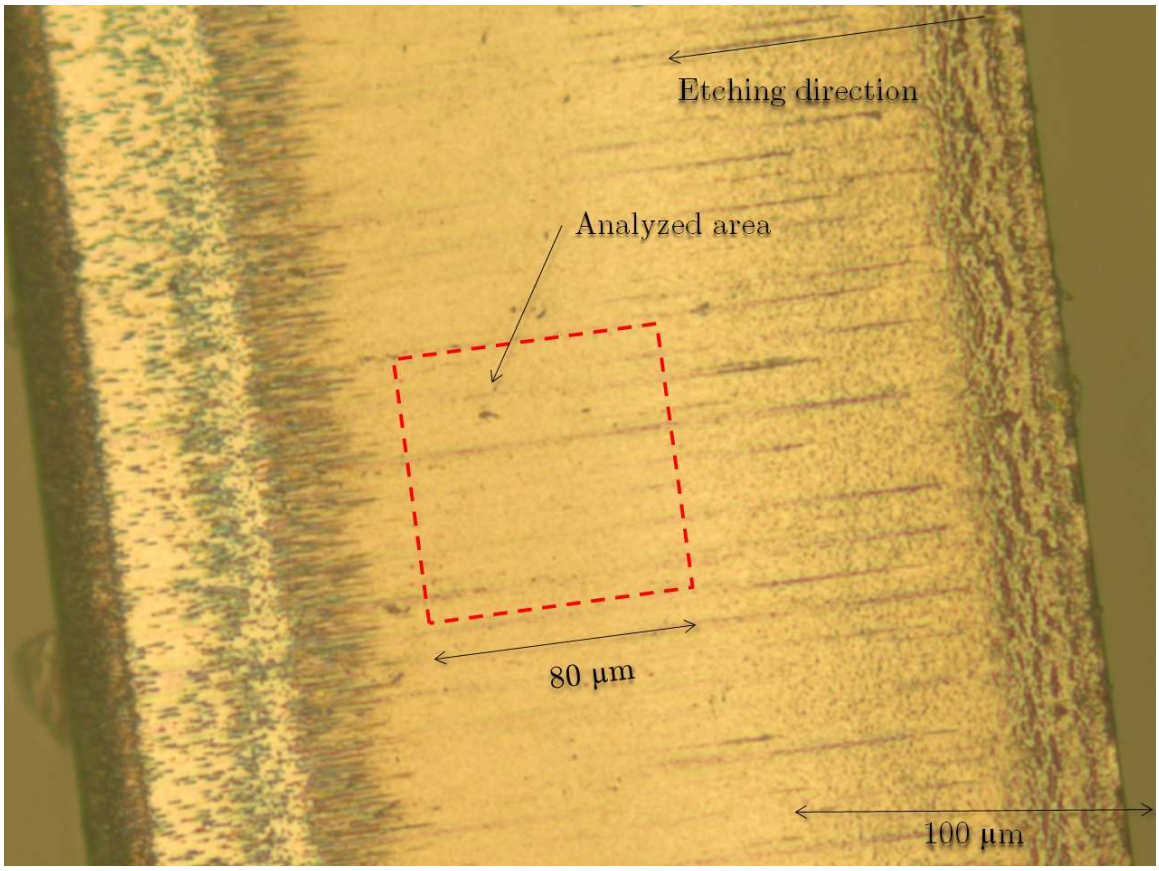

Figure 4-4. Micrograph of an unpolished DRIE-fabricated mirror chip micro-pore sidewall.

A listing of this testing plan is shown in Appendix A. The following sections will detail the experimental conditions and results from this series of tests.

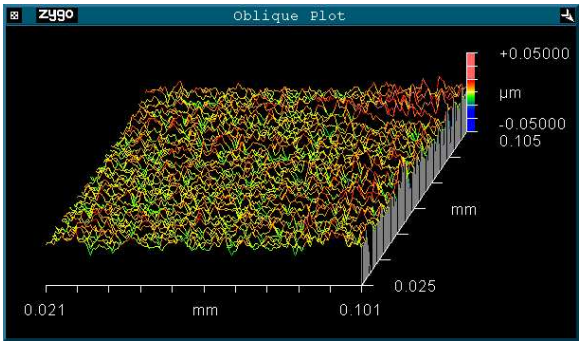

Figure 4-5. Three-dimensional shape of unpolished silicon mirror chip sidewall surface measured by an optical profilometer.

Table 4-1. Experimental conditions for abrasive size test.

Workpiece	Si mirror chip □ 7.5 × 0.2 mm
	Pore size 20 × 1500 μm
Abrasive slurry	Diamond slurry 0-0.5 μm, 0-0.2 μm,
	0.05 μm (mean diameter)
	Supplied amount: 1 mL
Magnetic fluid	Water based magnetic fluid
	Supplied amount: 1 mL
Pole - Pole distance	15 mm
Magnetic flux density	65.5 mT
Alternating current	1 A, 25 Hz
Polishing time	60 min

4.3.2 Effects of Diamond Slurries on Polishing Characteristics

Diamond slurries of three different sizes were chosen for this application. Table 4-1 lists the parameters used in this experiment to see the effects on surface roughness of different diamond slurries. Figure 4-6 contains two plots displaying the measured surface roughness under an automatic robust gauss spline (coarse, cutoff: 8 μm) filter and an averaging (fine, cutoff: 0.82 μm) filter. Figure 4-7 shows oblique plots of the measured surfaces after polishing with different abrasive slurries.

In Figure 4-6 a definite trend is observed in the coarse filtered plot. As the abrasive size increases, the roughness decreases. Under a coarse filter, larger abrasive particles will appear to remove larger surface errors. The roughness viewed under a fine filter however does not exhibit the same trend. The abrasive size seems to have no effect on the roughness at this scale.

4.3.3 Effects of Polishing Time on Polishing Characteristics

The effects of polishing time were examined. Table 4-2 shows the experimental conditions for this experiment. Figure 4-8 shows the roughness results under both a coarse and a fine filter. Figure 4-9 shows the surface profiler data for each polished mirror chip in the form of oblique plots.

Considering the coarse filter plot of Figure 4-8, the polishing process appears to not improve in surface roughness after 1 hour. The fine filter does not follow the same trend;

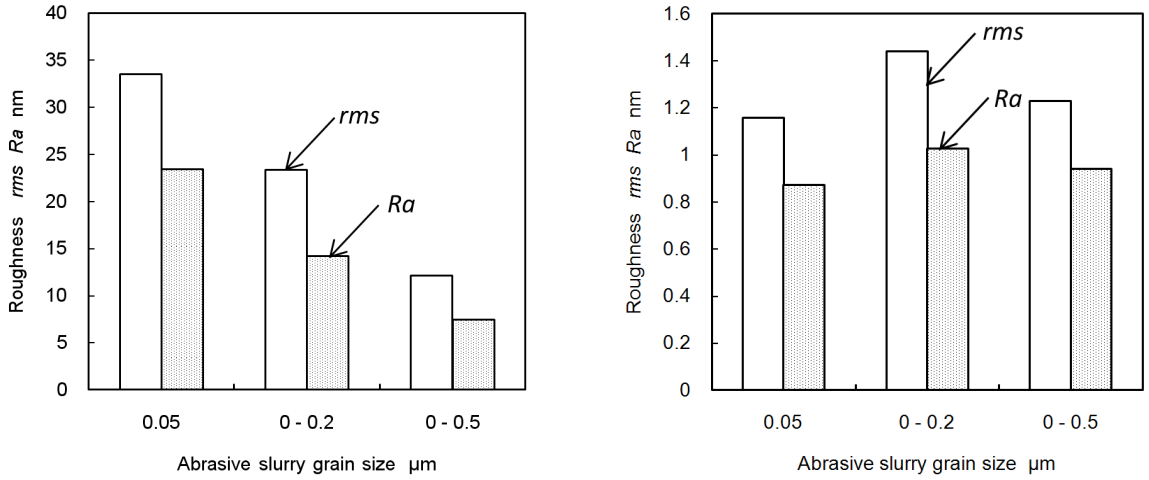

A Robust Gauss spline filter

B Averaging filter

Figure 4-6. Surface roughness results from abrasive size tests.

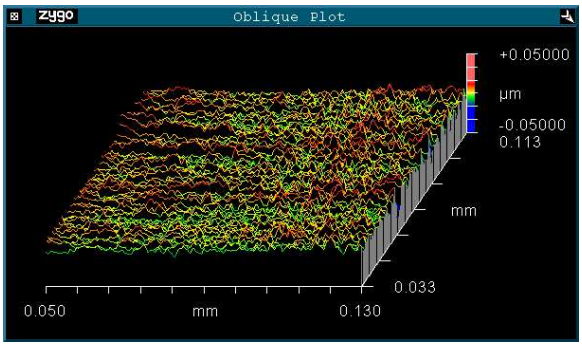

A Diamond slurry: 0.05 μm

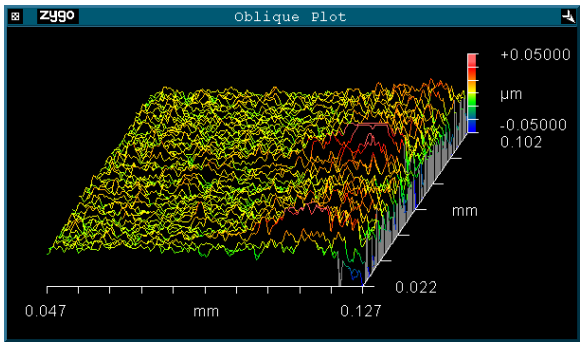

B Diamond slurry: 0 - 0.2 μm

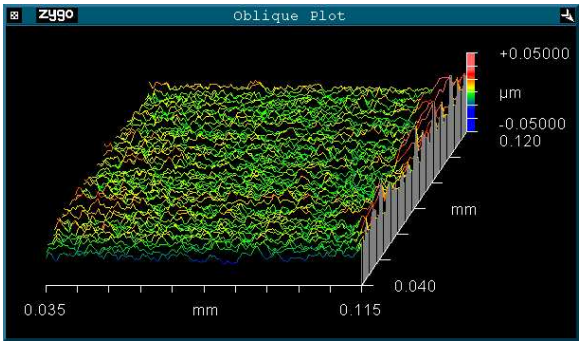

C Diamond slurry: 0 - 0.5 μm

Figure 4-7. Three-dimensional shape of silicon mirror chip micro-pore sidewall surfaces after abrasive size testing as measured by an optical profilometer.

Table 4-2. Experimental conditions for polishing time test.

Workpiece	Si mirror chip □ 7.5 × 0.2 mm
	Pore size 10 × 1500 μm
Abrasive slurry	Colloidal alumina suspension 0.05 μm
	(mean diameter)
	Supplied amount: 1 mL
Magnetic fluid	Water based magnetic fluid
	Supplied amount: 1 mL
Pole - Pole distance	15 mm
Magnetic flux density	65.5 mT
Alternating current	1 A, 25 Hz
Polishing time	30, 60, 120 min

however, those differences in roughness could be due to differences in the initial state of the wafer. Even with an indeterminate roughness trend under a fine filter, it seems as though 1 hour is sufficient to polish micro-pore sidewalls as most of the polishing seems to be accomplished in that amount of time.

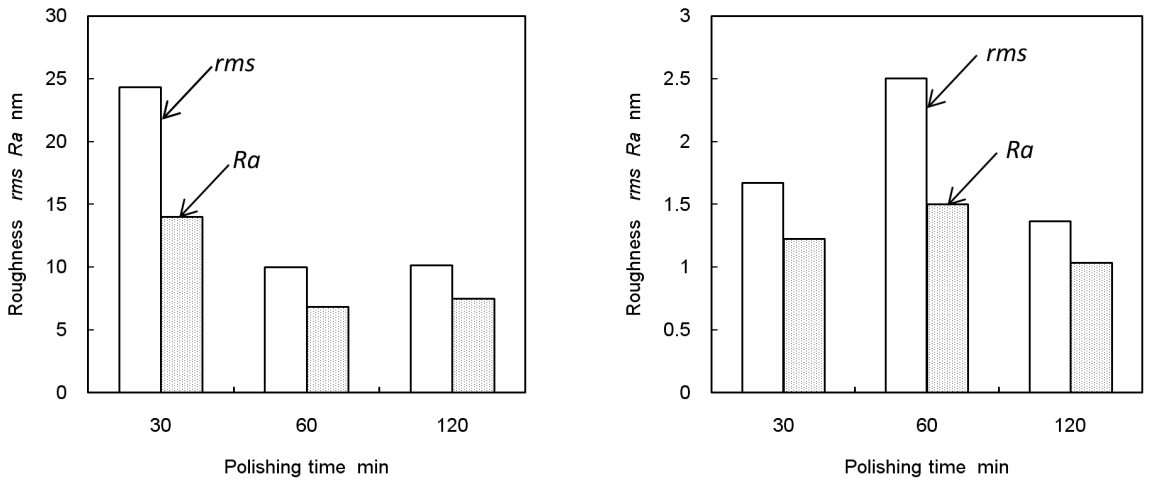

A Robust Gauss spline filter

B Averaging filter

Figure 4-8. Surface roughness results from polishing time tests.

4.3.4 Effects of Frequency of Magnetic Field on Polishing Characteristics

The effects on surface roughness of frequency of alternation of the magnetic field were examined. Table 4-3 shows the experimental conditions for this experiment. Figure

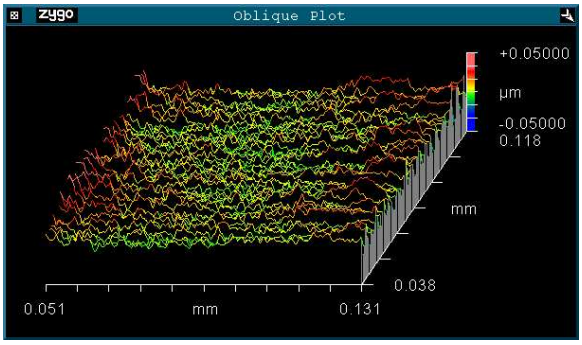

A Polishing time: 30 min

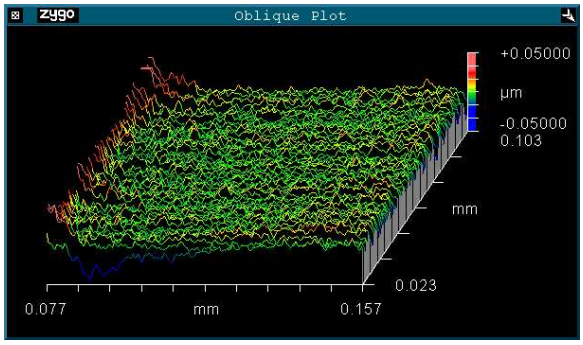

B Polishing time: 60 min

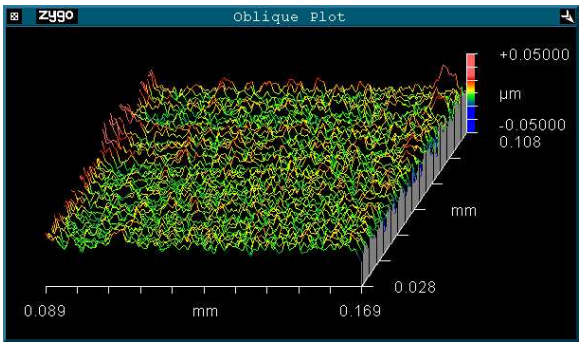

C Polishing time: 120 min

Figure 4-9. Three-dimensional shape of silicon mirror chip micro-pore sidewall surfaces after polishing time testing as measured by an optical profilometer.

Table 4-3. Experimental conditions for oscillating frequency test.

Workpiece	Si mirror chip □ 7.5 × 0.2 mm
	Pore size 20 × 1500 μm
Abrasive slurry	Diamond slurry 0.05 μm (mean diameter)
	Supplied amount: 1 mL
Magnetic fluid	Water based magnetic fluid
	Supplied amount: 1 mL
Pole - Pole distance	15 mm
Magnetic flux density	65.5 mT @ 25 Hz, 53.8 mT @ 50 Hz
Alternating current	1 A, 25, 50 Hz
Polishing time	60 min

4-10 shows the roughness results under both coarse and fine filters. Figure 4-11 shows the surface profiler data for each polished mirror chip in the form of oblique plots.

The fluid, like any physical system, responds to an external stimulus which is, in this case, the alternating magnetic field. At low frequencies (1 - 10 Hz) the fluid exhibits a uni-modal response. At higher frequencies (over 10 Hz) the fluid develops secondary and

tertiary modes of vibration (multi-modal response). However, when the forcing frequency continues to rise, the amount of fluid agitation drops drastically until it does not move at all. Under these conditions, the fluid must not have been agitated enough to create relative motion between it and the sidewall surface.

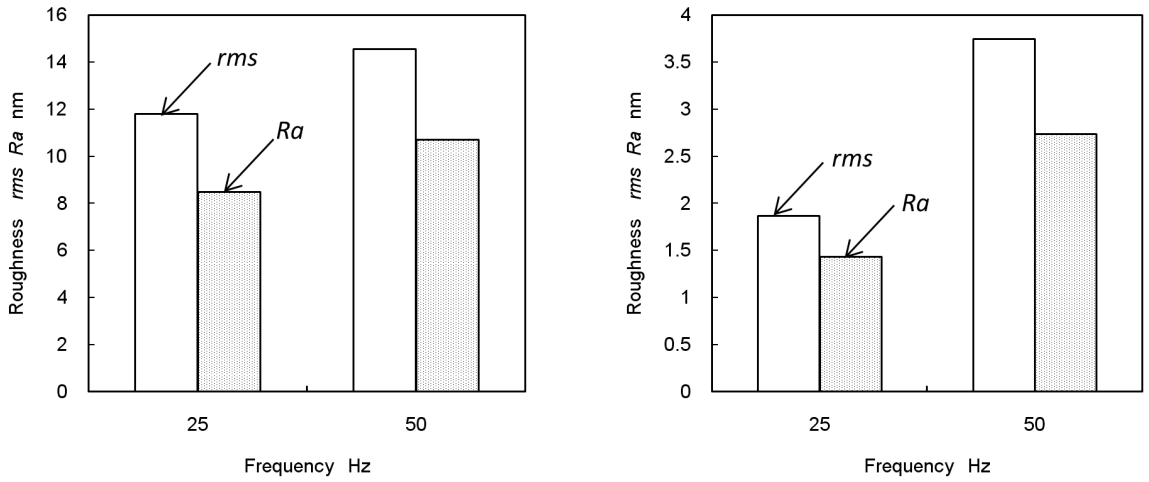

A Robust Gauss spline filter

B Averaging filter

Figure 4-10. Surface roughness results from frequency variation tests.

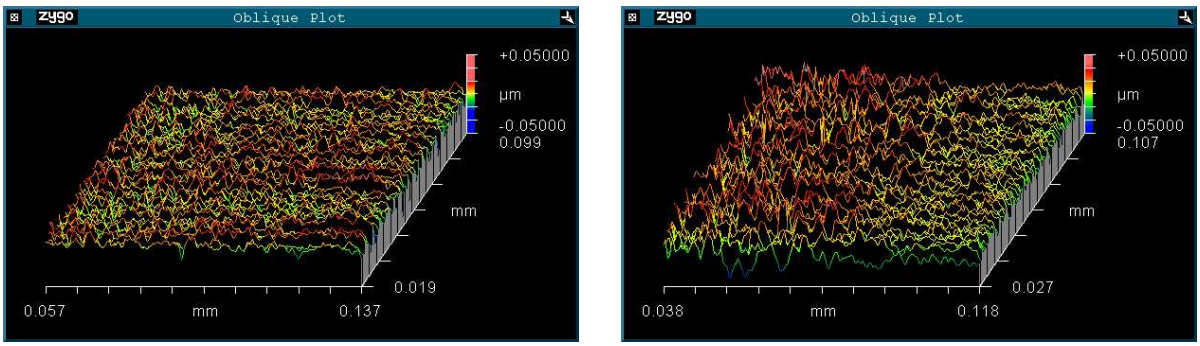

A Frequency: 25 Hz

B Frequency: 50 Hz

Figure 4-11. Three-dimensional shape of silicon mirror chip micro-pore sidewall surfaces after frequency variation testing as measured by an optical profilometer.

4.3.5 Effects of Micro-pore Width on Polishing Characteristics

The effects on surface roughness of the micro-pore's width were examined. Table 4-4 lists the experimental conditions for this experiment. Figure 4-12 shows the roughness

Table 4-4. Experimental conditions for micro-pore width test.

Workpiece	Si mirror chip □ 7.5 × 0.2 mm
	Pore size 10 × 1500, 20 × 1500,
	50 × 1500 μm
Abrasive slurry	Diamond slurry 0.05 μm (mean diameter)
	Supplied amount: 1 mL
Magnetic fluid	Water based magnetic fluid
	Supplied amount: 1 mL
Pole - Pole distance	15 mm
Magnetic flux density	65.5 mT
Alternating current	1 A, 25 Hz
Polishing time	60 min

results under both a coarse and a fine filter. Figure 4-13 shows the surface profiler data for each polished mirror chip in the form of oblique plots.

There is not a clear trend in the coarse filtered roughness values. However, the fine filtered roughness values do show a trend. Apparently, smaller slit width yields better small scale roughness. This occurrence could be due to the fact that in the experiment, the fluid oscillated at the same velocity for all three mirror chips. When the fluid impinges on the mirror chip face, the fluid is both pressured by fluid momentum and pulled by magnetic force through the micro-pores. The magnetic abrasive fluid would flow faster through the micro-pores of reduced sized than through larger micro-pores. Faster fluid flow would yield a more efficient polishing process with higher finishing forces and would leave a better surface.

4.3.6 Effects of Chemical Assistance on Polishing Characteristics

The abrasive used in this experiment was colloidal silica which is a suspension of silica particles in water and other chemicals having a high pH (alkaline). Colloidal silica is often used as a final step in polishing silicon wafers to angstrom order surface roughness for the semiconductor industry. It works not by mechanical abrasion but by chemical dissolution and mechanical removal of the chemical reaction products, a process called chemical mechanical polishing (CMP). Simply stated, silica particles in the alkaline solution bond with the open bonds of surface atoms of the silicon substrate. The particle

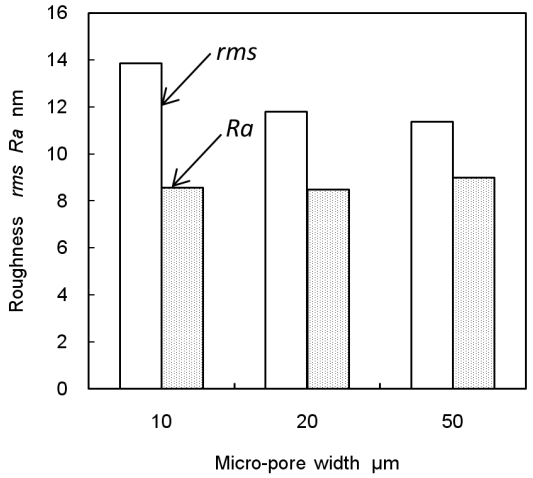

A Robust Gauss spline filter

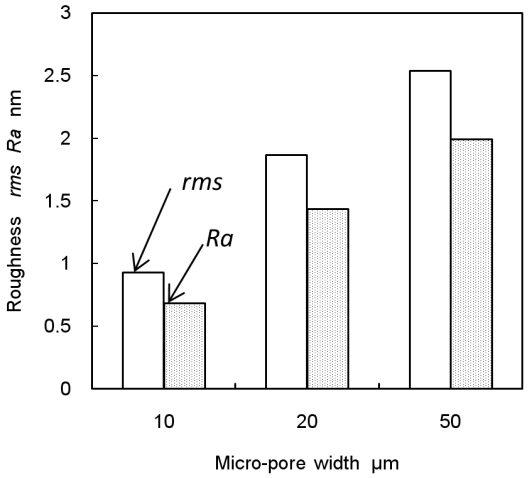

B Averaging filter

Figure 4-12. Surface roughness results from micro-pore width tests.

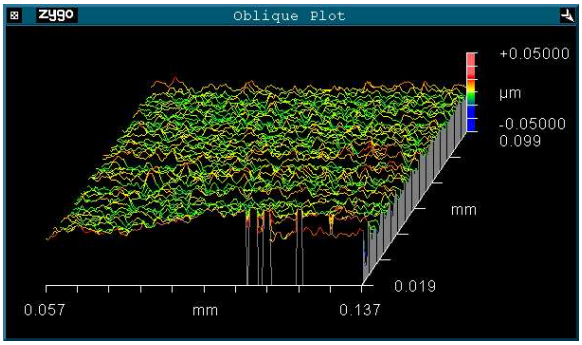

A Micro-pore width: 10 μm

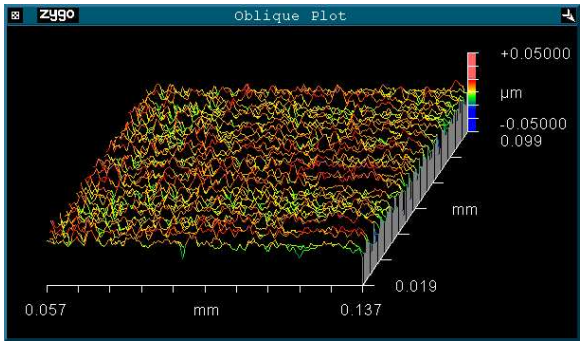

B Micro-pore width: 20 μm

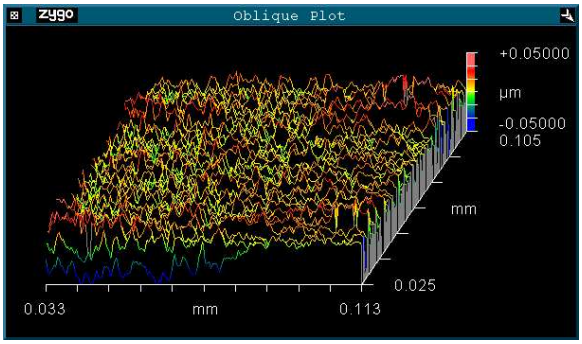

C Micro-pore width: 50 μm

Figure 4-13. Three-dimensional shape of silicon mirror chip micro-pore sidewall surfaces after micro-pore width variation testing as measured by an optical profilometer.

Table 4-5. Experimental conditions for chemical assistance test.

Workpiece	Si mirror chip □ 7.5 × 0.2 mm
	Pore size 20 × 1500 μm
Abrasive slurry	Colloidal Silica 40 - 50 nm mean diameter
	Supplied amount: 1 mL
Magnetic fluid	Water based magnetic fluid
	Supplied amount: 1 mL
Pole - Pole distance	15 mm
Magnetic flux density	65.5 mT
Alternating current	1 A, 25 Hz
Polishing time	60 min

is then attached to the substrate atoms. Mechanical action from a polishing pad removes the attached silica particle and the silicon atoms to which it was bonded. This mechanism of material removal allows it to be extremely precise as it literally removes a single layer of atoms at a time[26]. It was thought that perhaps using colloidal silica to polish the silicon mirror chips could yield lower surface roughness. The use of colloidal silica in these tests is dubbed "chemical assistance" for the purpose of this document.

The effects on surface roughness of chemical assistance were examined. Table 4-5 lists the experimental conditions for this experiment. Figure 4-14 shows the roughness results under both a coarse and a fine filter. Figure 4-15 shows the surface profiler data for each polished mirror chip in the form of oblique plots.

It is difficult to state if a trend exists from these two trials. It is also difficult to state whether any material was removed at all. The silica particles should have a hardness similar to that of the silicon mirror chip. Therefore, if any material removal occurs, it is unlikely that it is a result of mechanical removal and very likely that it was the result of chemical action. Also, in commercial polishing application that use colloidal silica, it is only used as a final step to reduce the surface roughness of silicon wafers from a few nanometers to less than 1 nm; in other words, it is used to remove small wavelength surface errors in the target surface[26]. In the coarse plot of Figure 4-14, a change in surface roughness is seen; however, since CMP is believed to only affect small wavelength surface errors, one must assume that the process had no effect under this filter and that the

change is surface roughness is simply due to a difference in initial state of the two wafers used for this test.

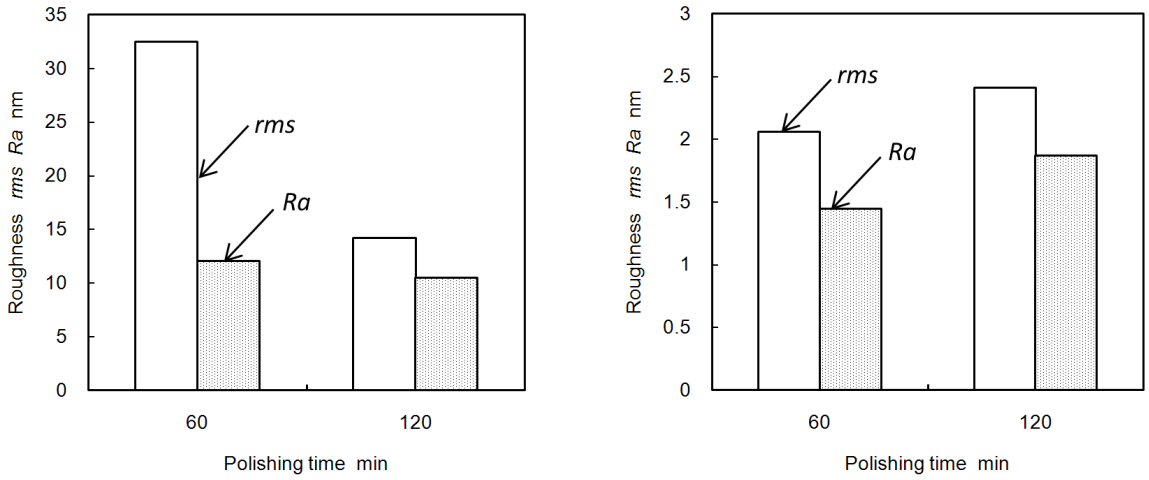

A Robust Gauss spline filter

B Averaging filter

Figure 4-14. Surface roughness results from chemical assistance tests.

The fine plot of Figure 4-14 shows a small change in roughness. However, this change (about 0.3 nm *rms*) is not enough to declare as the result of the polishing process for two reasons. First, the roughness at 2 hours of polishing is actually higher than the roughness at 1 hour which is an unexpected and unintuitive result. Second, since the difference in roughness under the coarse filter of the two mirror chips used to run this experiment is so drastic (>15 nm *rms*), one should assume that the roughness of the two mirror chips under fine filter would be also be incomparable. The results from this test are therefore inconclusive and require further study. Unfortunately, due to the limited number of workpieces, further testing was not possible.

4.4 LIGA-Fabricated Mirrors

4.4.1 Unpolished State

The initial state of unpolished micro-pore sidewalls of nickel mirror chips fabricated by x-ray LIGA differs from sample to sample much less than that of DRIE-fabricated wafers. The average surface roughness of the micro-pore sidewalls in nickel mirror chips

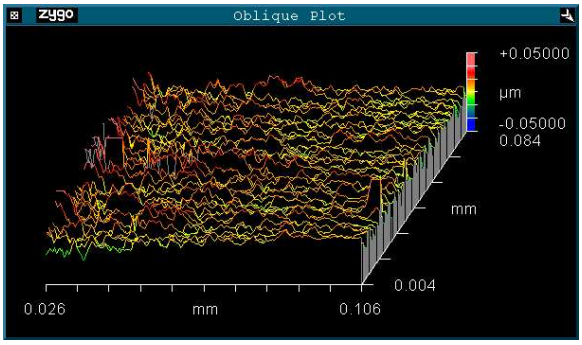

A Polishing time: 60 min

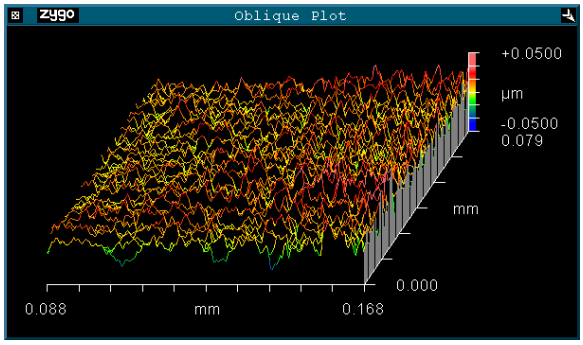

B Polishing time: 120 min

Figure 4-15. Three-dimensional shape of silicon mirror chip micro-pore sidewall surfaces after chemical assistance testing as measured by an optical profilometer.

is 13 nm *rms*. Also, the overall shape of the sidewall surface tends to be very flat whereas the sidewalls of DRIE-fabricated micro-pores often have some curvature throughout the thickness of the mirror chip. Figure 4-16 shows both an oblique plot of the surface of one micro-pore and an intensity map of the same data. A periodic texture is seen.

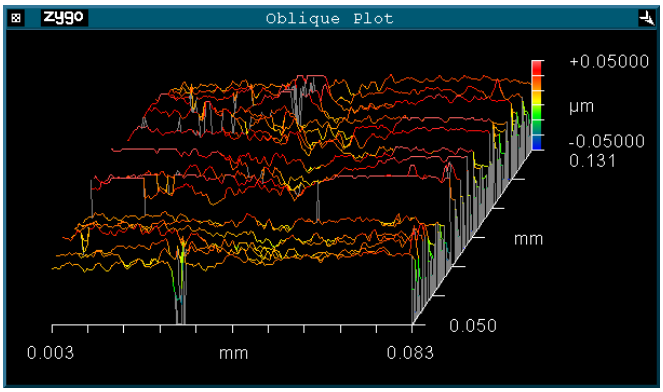

A Oblique plot

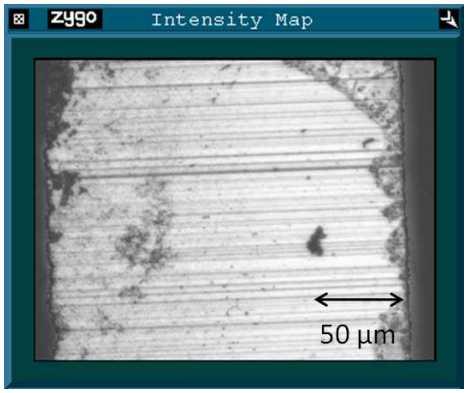

B Intensity map

Figure 4-16. Optical profilometer data for an unpolished mirror chip.

The fact that LIGA-fabricated mirror chips are made of nickel is more promising, as nickel is softer than silicon; having a softer substrate material is typically a disadvantage in a polishing processes as plowing and rubbing occurs more often at the abrasive cutting edge-workpiece interface than with harder materials. However, since this process seems to apply minimal force, the polishing process was expected to work more efficiently.

Table 4-6. Experimental conditions for nickel mirror chip trial.

Workpiece	Ni mirror chip □ 7.5 × 0.2 mm
	Pore size 20 × 2000 μm
Abrasive slurry	Diamond slurry 0-0.5 μm
	Supplied amount: 1 mL
Magnetic fluid	Water based magnetic fluid
	Supplied amount: 1 mL
Pole - Pole distance	15 mm
Magnetic flux density	65.5 mT
Alternating current	1 A, 25 Hz
Polishing time	60 min

Only two LIGA-fabricated mirror chips were provided. A full testing sequence was therefore not possible. Instead, a single trial was executed. The parameters for this test were chosen based on the results from the testing done on DRIE-fabricated mirror chips. The chosen parameters were ones that seem to yield the best results such as 1 hour polishing time, 0 - 0.5 μm diamond slurry, 25 Hz oscillation frequency.

4.4.2 Polishing Characteristics

Table 4-6 lists the experimental conditions for this polishing trial. Figure 4-18 shows the roughness results under both a coarse and a fine filter. Figure 4-17 shows the surface profiler data for the polished wafer in the form of an oblique plot of the surface and an intensity map.

According to the data, this test was undeniably successful. Figure 4-18 shows a definite change in roughness under both coarse and fine filters. There is clear evidence of material removal in intensity maps of Figures 4-18 and 4-16. In step 7 of Figure 1-11, the final workpiece is shown to have a thin gold plating on all vertical surfaces; this implies that the surface seen in the intensity map of Figure 4-16 is gold. The intensity map of Figure 4-17 shows dark areas and light areas; where the light areas are presumed to be made of gold and the darker areas are presumed to be where the underlying nickel has been exposed. Clearly, more polishing time is required to fully remove the gold layer,

as it would interfere with the mirror chip's x-ray reflection properties, but this test demonstrates that this process is in fact able to polish micro-pore sidewalls.

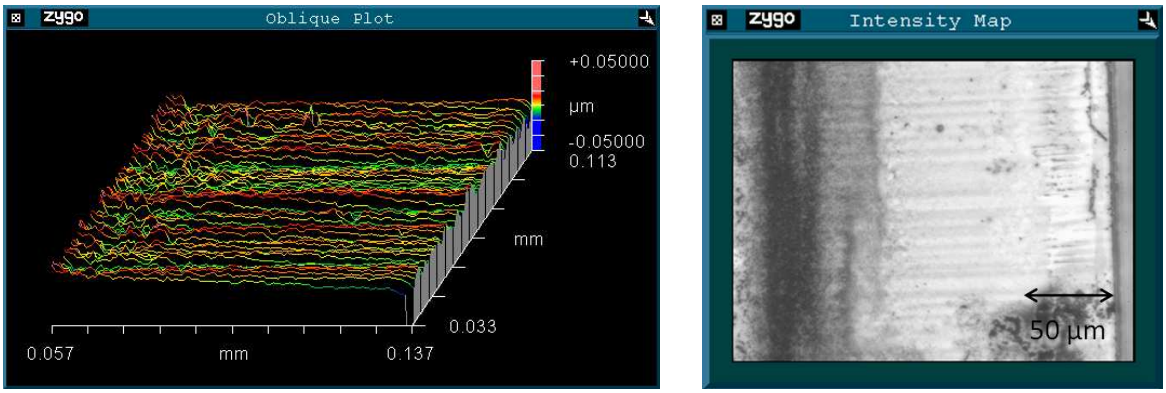

A Oblique plot

B Intensity map

Figure 4-17. Optical profilometer data for a polished mirror chip.

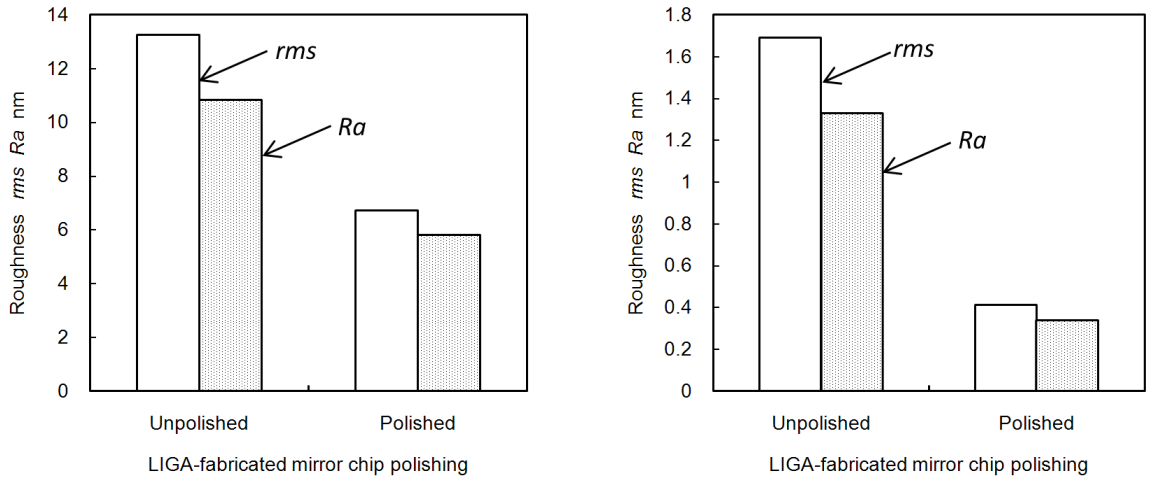

A Robust Gauss spline filter

B Averaging

Figure 4-18. Comparison of sidewall surface roughness before and after polishing.

CHAPTER 5
X-RAY REFLECTION TESTING

5.1 Testing Method

To test the x-ray reflectance of a mirror chip means to verify the intensity of any reflected x-ray radiation. Figure 5-1 is a schematic of the testing setup. Essentially, a collimated beam of x-rays is aimed at the mirror chip, whose micro-pore sidewalls are initially parallel with the incident beam. The incident angle, in this case, is the acute angle between the x-rays and the micro-pore sidewall surface. The mirror chip is slowly rotated until the x-rays are obscured. The intensity of the reflected x-rays is measured by a detector directly behind the mirror chip.

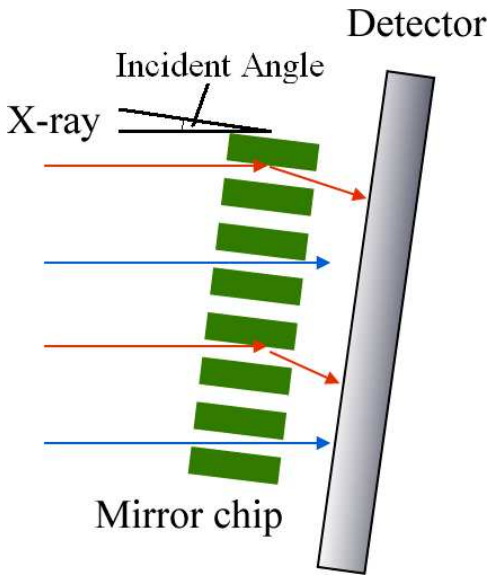

Figure 5-1. Schematic of x-ray reflectance testing setup for micropore mirror chips.

Figure 5-2 has a photograph of an outer view of the testing device at JAXA. The inside of this device is held at a vacuum during testing to minimize the absorption of x-rays into air. The left half of Figure 5-2 is a schematic of the testing device. As shown in the schematic, the left area is where the x-rays are generated. The x-rays are collimated by passing through a pin-hole opening. They then travel down a vacuum pipe through another pin-hole for further collimation. The mirror chip is mounted on a 2 axis goniometer which is then mounted onto a three axis stage (not labeled). Since the x-ray

beam is passed through small pin-holes, only a small area of the mirror chip is used to check the reflectance.

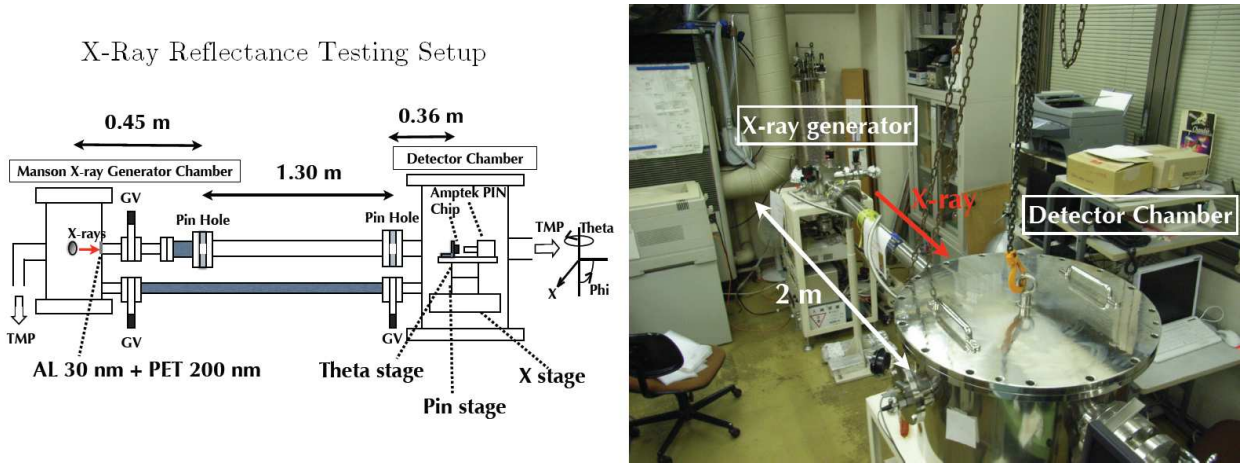

Figure 5-2. X-ray reflectance testing setup.

Data from the test is then plotted. If there the mirror chip exhibited no x-ray reflection, a linear drop in intensity versus incident angle will be observed due to the mirror chip's geometry. If the mirror-chip did reflect x-rays, an excess in intensity at small angles ($< 2°$) would have been observed.

5.2 Grazing Incidence X-Ray Scattering and Specular Reflectance Test Results

This test was performed to verify the mirror chips' ability to achieve specular reflectance of x-rays at grazing incidence. Therefore, the type of testing performed is called "grazing incidence x-ray specular reflectance testing." Measured values for the micro-pore sidewall roughness of LIGA-fabricated mirror chips in their unpolished state were consistently above 10 nm *rms*. Such a high roughness would not reflect x-rays; therefore the reflectance test was not performed on an unpolished LIGA-fabricated mirror chip.

Figure 5-3 shows the reflection data for a polished LIGA-fabricated nickel mirror chip. In Figure 5-3, the excess in intensity due to x-ray reflection of the sidewalls is labeled; the

points clearly follow the 4 nm *rms* theoretical intensity profile. This result demonstrates the polishing process' ability to improve the x-ray reflection performance of mirror chips.

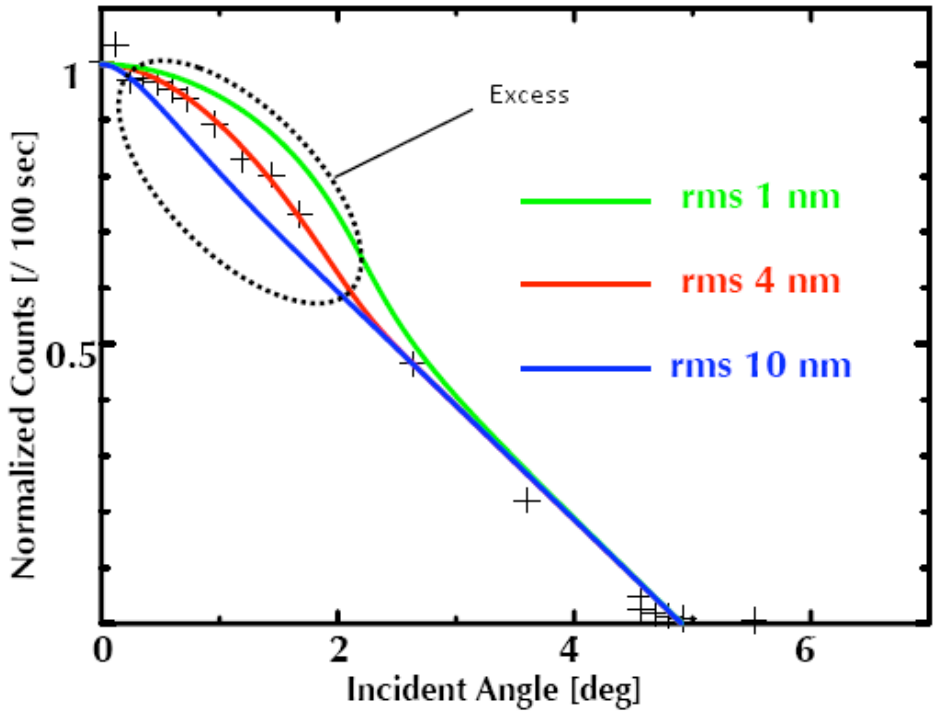

Figure 5-3. X-ray reflectance data for a polished nickel mirror chip.

CHAPTER 6
CONCLUSIONS

6.1 Concluding Statements

This research examined the need for and development of a new magnetic field assisted finishing process as applied to the finishing of micro-pore optics. A preliminary understanding of the finishing mechanisms was established through a set of finishing experiments. The results from this work may be summarized in the following statements:

1. A new finishing process for improving the surface roughness of micro-pore sidewalls was conceived, and its processing principle was defined according to an assessment of the workpiece dimensions and prior surface engineering knowledge.

2. A machine was developed to materialize the processing principle. For a ferrous fluid to materialize the processing principle, it must have low magnetic force and low viscosity such that the fluid dynamic motion, encouraging relative motion between the abrasive particles and the micro-pore wall surface.

3. The finishing characteristics of the polishing process were studied through a series of polishing experiments. The effects on surface roughness of process parameters were studied; these included abrasive size, frequency of magnetic field oscillation, polishing time, and chemical assistance.

4. The mechanism by which material removal occurs was determined by observations preliminary trials. It was noticed that the principal agent determining the success of a polishing trial was the magnetic abrasive fluid's dynamic motion. Fluid agitation (dynamic motion) was found to be primarily controlled by the frequency of magnetic field oscillation and the magnetic field strength.

5. X-ray reflection tests demonstrated the polishing process' effectiveness in improving the x-ray reflectivity of mirror-chips.

6.2 Future Work

This research is a preliminary step in only one facet of the effort to realize an ultra-lightweight and high resolution micro-pore x-ray telescope. The achievement of such a telescope will be the result of the combined efforts of several institutions. Their success in tackling their individual challenges with the development of this telescope will ultimately determine whether the project is successful or not. As stated, a crucial step in the telescope's development is lowering the sidewall surface roughness of micro-pore

sidewalls full-size x-ray mirrors to an acceptable level. For this goal, the new polishing process presented in this research will need to be developed and controlled; however, this is certainly not the only application for which the new polishing process is well suited. In the field of MEMS, situations may arise in which imperfections of feature geometry may need correction by a process such as this new polishing process. In ultra-precision polishing applications, this polishing process, which is based on the controllable yet gentle forces of MF, may find a use as a final phase of polishing.

This new polishing process' feasibility for future applications will depend on both its further development and in the understanding of its process specific trends. Analytical, empirical, and theoretical models may need to be established; however, this polishing process is, in fact, new, as there is no other polishing process in existence that employs the dynamic motion of an MF-based magnetic abrasive fluid actuated by an alternating magnetic field to cause material removal.

Tasks required in the immediate future of this research involve the running of a more elaborate, thorough and statistically sound testing sequence to verify the effects of varying process parameters with a higher level of confidence. Hopefully, useful trends will be determined. Also a new machine, capable of polishing full-size micro-pore x-ray mirrors, will need to be developed.

This new machine design will greatly improve on the machine used for this research. One major problem is the overheating of the electromagnets allowing the machine to run just 1 hour at a time. This problem shall be overcome through several approaches. Instead of solid steel magnetic components, laminated steel shall be used; this is a common technique in industry. Greater care will be used in the winding of the coils for the electromagnets. Also, a closed loop water cooling system will be implemented into the new design. These measures should allow the new machine to run for extended periods of time (days). A computer controlled motion and power control system shall be integrated into

the design of the new machine to both hold and rotate the full-size optic, as it can only be polished in sections.

Once the full-size micro-pore x-ray mirrors meet design specifications, the telescope, for which these optics are intended, shall be prototyped. It is hoped that the development of this telescope will eventually lead to it being launched into space for a successful mission.

This research has explored a new area of polishing technology; this was a challenging task because there was often no reference by which to make an educated decisions. Often, decisions were made based simply on intuition. It is hoped that this work will serve as a reference point for future research on this topic and that use of this technology can help render new x-ray telescopes to study objects in deep space, improving mankind's knowledge of physics and the universe.

APPENDIX: TESTING PLAN

Table A-1. Experimental conditions for each test on silicon mirror chips.

Test	Test variable	Abrasive slurry	Time hr	Frequency Hz	Pore orientation
1	Time	0.05 μm Colloidal Alumina	0.5	25	Horizontal
2	Time	0.05 μm Colloidal Alumina	1	25	Horizontal
3	Time	0.05 μm Colloidal Alumina	2	25	Horizontal
4	Orientation	0.05 μm Diamond Slurry	1	25	Horizontal
5	Orientation	0.05 μm Diamond Slurry	1	25	Vertical
6	Slit Width	0.05 μm Diamond Slurry	1	25	Horizontal
7	Slit Width	0.05 μm Diamond Slurry	1	25	Horizontal
8	Slit Width	0.05 μm Diamond Slurry	1	25	Horizontal
9	Frequency	0.05 μm Diamond Slurry	1	25	Horizontal
10	Frequency	0.05 μm Diamond Slurry	1	50	Horizontal
11	Abrasive Size	0.05 μm Diamond Slurry	1	25	Horizontal
12	Abrasive Size	0 - 0.2 μm Diamond Slurry	1	25	Horizontal
13	Abrasive Size	0 - 0.5 μm Diamond Slurry	1	25	Horizontal
14	CMP Time	40-50 nm Colloidal Silica	1	25	Horizontal
15	CMP Time	40-50 nm Colloidal Silica	2	25	Horizontal

Table A-2. Silicon mirror chips used for testing and their micro-pore dimensions.

Test	Pore width μm	Pore spacing μm	Radius mm
1	10	300	50
2	10	300	150
3	10	300	250
4	50	100	150
5	50	100	250
6	10	50	150
7	20	50	150
8	50	50	250
9	20	50	150
10	20	100	50
11	10	50	50
12	10	50	250
13	10	100	50
14	20	300	250
15	20	200	250

Table A-3. Surface roughness values of silicon mirror chip micro-pore sidewalls

	Large filter		Fine Filter	
Test	*rms* nm	*Ra* nm	*rms* nm	*Ra* nm
1	24.341	14.013	1.67	1.223
2	9.971	6.844	2.505	1.5
3	10.117	7.494	1.363	1.035
4	14.63	10.196	3.598	2.432
5	16.593	10.05	3.155	2.231
6	13.868	8.559	0.93	0.682
7	11.786	8.484	1.866	1.433
8	11.371	8.99	2.54	1.992
9	11.786	8.484	1.866	1.433
10	14.545	10.682	3.748	2.731
11	33.509	23.4	1.156	0.872
12	23.362	14.183	1.44	1.026
13	12.117	7.457	1.227	0.942
14	32.434	12.04	2.06	1.448
15	14.213	10.475	2.408	1.868

REFERENCES

[1] "X-ray astronomy," (September 2004). http://imagine.gsfc.nasa.gov/docs/science/know_l2/history_xray.html.

[2] Ezoe, Y., Mitsuisi, I., Takagi, U., Ishida, M., Mitsuda, K., Yamasaki, N., Shirata, T., Ohashi, T., Fujiwara, K., Morishita, K., Nakajima, K., Fujihira, S., Kanamori, Y., Riveros, R., Yamaguchi, H., Kato, F., Sugiyama, S., and Maeda, R., "Development of light-weight & high-resolution x-ray pore optics in japan," International Workshop on Astronomical X-ray Optics (December 2008).

[3] Tipler, P. A. and Mosca, G., [*Physics for scientist and engineers, Volume 2*], Worth Publishers, New York (1995).

[4] Spiller, E., "X-ray optics," *Advances in x-ray analysis* **42**, 297–307 (2000).

[5] Petre, R., "X-ray imaging systems," (September 2004). http://imagine.gsfc.nasa.gov/docs/science/how_l2/xtelescopes_systems.html.

[6] "Chandra x-ray observatory," (July 1999). http://www.shuttlepresskit.com/STS-93/payload45.htm.

[7] "Suzaku: The x-ray relescope," (June 2005). http://imagine.gsfc.nasa.gov/docs/features/exhibit/astroe2_xray_telescope.html.

[8] Ezoe, Y., Koshiishi, M., Mita, M., Mitsuda, K., Hoshino, A., Ishisaki, Y., Yang, Z., Takano, T., and Maeda, R., "Micropore x-ray optics using anisotropic wet etching of (110) silicon wafers," *Applied Optics* **45**(35), 8932–8938 (2006).

[9] Marxer, C., Thio, C., Gretillat, M.-A., de Rooij, N. F., Battig, R., Anthamatten, O., Valk, B., , and Vogel, P., "Vertical mirrors fabricated by deep reactive ion etching for fiber-optic switching applications," *Journal of Microelectromechanical Systems* **6**(3), 227–285 (1997).

[10] Carlo, F. D., Mancini, D., Lai, B., and Song, J., "Characterization of exposure and processing of thick pmma for deep x-ray lithography using hard x-rays," *Microsystem Technologies* **4**, 86–88 (1998).

[11] Becker, H. and Heim, U., "Hot embossing as a method for the fabrication of polymer high aspect ratio structures," *Sensors and Actuators* **83**, 130–135 (2000).

[12] Baron, Y. M., [*Technology of abrasive machining in a magnetic field*], Masino-strojenije, Leningrad, Russia (1975).

[13] Yamaguchi, H., [*Handbook of lapping and polishing*], CRC Press, Boca Raton, Florida (2007).

[14] Ruben, H., [*Advances in Surface Treatments*], Pergamon Press, Oxford (1987).

[15] Shinmura, T. and Yamaguchi, H., "Study on a new internal finishing process by the application of magnetic abrasive machining(internal finishing of stainless steel tube and clean gas bomb)," *JSME International Journal, Series C* **38**(4), 798–804 (1995).

[16] Yamaguchi, H., Yumoto, K., Shinmura, T., and Okazaki, T., "Study of finishing wafers by magnetic field assisted finishing," *Journal of Advanced Mechanical Design, Systems, and Manufacturing* **3**(1), 35–46 (2009).

[17] Mahalik, N., [*Micromanufacturing and nanotechnology*], Springer, Germany (2006).

[18] Svoboda, J., [*Magnetic techniques for the treatment of materials*], Kluwer Academic Publishers, The Netherlands (2004).

[19] Kordonski, W. and Golini, D., "Fundamentals of magnetorheological fluid utilization in high precision finishing," *Journal of Intelligent Material Systems and Structures* **10**, 683–689 (1999).

[20] Kurobe, T., Imanaka, O., and Tachibana, S., "Magnetic field-assisted fine finishing," *Bulletin of the Japan Society of Precision Engineering* **17**(1), 49–50 (1983).

[21] Yamaguchi, H., Shinmura, T., and Sekine, M., "Uniform internal finishing of sus304 stainless steel bent tube using a magnetic abrasive finishing process," *ASME Journal of Manufacturing Science and Engineering* **127**, 605–611 (2005).

[22] Yamaguchi, H., Shinmura, T., and Ikeda, R., "Study of internal finishing of austenitic stainless steel capillary tubes by magnetic abrasive finishing," *ASME Journal of Manufacturing Science and Engineering* **129**, 885–892 (2007).

[23] Yamaguchi, H., Shinmura, T., and Takenaga, M., "Development of a new precision internal machining process using an alternating magnetic field," *Precision Engineering* **27**, 51–58 (2003).

[24] Nakajima, K., Fujiwara, K., Pan, W., and Okuda, H., "Shaped silicon-crystal wafers obtained by plastic deformation and their application to silicon-crystal lenses," *Nature Materials* **4**, 47–50 (2005).

[25] Bennett, J. M., [*Light Scattering and Nanoscale Surface Roughness*], Springer, New York (2007).

[26] Doi, T. K., [*Handbook of Lapping and Polishing*], CRC Press, Boca Raton, Florida (2007).

BIOGRAPHICAL SKETCH

Raúl Riveros was born in 1985 in the city of Maracay, Venezuela, to Ivan and Angelica Riveros. He and his family came to the United States in 1992, and he has lived in Florida ever since. He joined the University of Florida in 2005 and graduated with a Bachelor of Science in mechanical engineering in 2007. As an undergraduate, Raúl conducted research at the Machine Tool Research Center (MTRC). He started his graduate work under the guidance of Dr. Hitomi Yamaguchi Greenslet in January of 2008 and graduated with a Master of Science in mechanical engineering in May 2009 from the University of Florida.